

Cell Biology:

**Nrbf2 Suppresses Autophagy by
Modulating Atg14L-containing Beclin
1-Vps34 Protein Complex Architecture and
Reducing Intracellular
Phosphatidylinositol-3 Phosphate Levels**

Yu Zhong, Deanna H. Morris, Lin Jin, Mittul
S. Patel, Senthil K. Karunakaran, You-Jun Fu,
Emily A. Matuszak, Heidi L Weiss, Brian T.
Chait and Qing-Jun Wang
J. Biol. Chem. published online August 1, 2014



Access the most updated version of this article at doi: [10.1074/jbc.M114.561134](https://doi.org/10.1074/jbc.M114.561134)

Find articles, minireviews, Reflections and Classics on similar topics on the [JBC Affinity Sites](http://www.jbc.org/).

Alerts:

- [When this article is cited](#)
- [When a correction for this article is posted](#)

[Click here](#) to choose from all of JBC's e-mail alerts

This article cites 0 references, 0 of which can be accessed free at
<http://www.jbc.org/content/early/2014/08/01/jbc.M114.561134.full.html#ref-list-1>

Title page

Title: Nrbf2 Suppresses Autophagy by Modulating Atg14L-containing Beclin 1-Vps34 Protein Complex Architecture and Reducing Intracellular Phosphatidylinositol-3 Phosphate Levels

Yu Zhong¹, Deanna H. Morris¹, Lin Jin¹, Mittul S. Patel¹, Senthil K. Karunakaran¹, You-Jun Fu¹, Emily A. Matuszak², Heidi L. Weiss³, Brian T. Chait⁴, Qing Jun Wang^{1,2,3,5}

¹ Department of Molecular and Cellular Biochemistry, University of Kentucky, Lexington, KY 40536, USA.

² Graduate Center for Toxicology, University of Kentucky, Lexington, KY 40536, USA.

³ Markey Cancer Center, University of Kentucky, Lexington, KY 40536, USA.

⁴ Laboratory of Mass Spectrometry and Gaseous Ion Chemistry, Rockefeller University, New York, NY 10065, USA.

⁵ Correspondence: Department of Molecular and Cellular Biochemistry, University of Kentucky College of Medicine, B163 BBSRB, 741 South Limestone, Lexington, KY 40536, USA. Email: qingjun.wang@uky.edu.

Running Title: Autophagy Regulation by Nrbf2

Keywords: autophagy, protein-protein interactions, cellular regulation, protein degradation, subcellular organelles, Beclin 1, Vps34, Nrbf2, autophagosome biogenesis

Capsule

Background: The Beclin 1-Vps34 protein-protein interaction network is critical for autophagy regulation.

Results: Nrbf2 is a component of the Atg14L-containing Beclin 1-Vps34 protein complex; Nrbf2 deficiency disrupts Atg14L-Vps34/Vps15 interactions and increases intracellular PI3P levels and autophagic flux.

Conclusion: Nrbf2 is important for the Beclin 1-Vps34 interaction network to achieve tight autophagy regulation.

Significance: Our work identifies a novel aspect of autophagy regulation.

Abstract

Autophagy is a tightly regulated lysosomal degradation pathway for maintaining cellular homeostasis and responding to stresses. Beclin 1 and its interacting proteins, including the class III phosphatidylinositol-3 kinase Vps34, play crucial roles in autophagy regulation in mammals. We identified nuclear receptor binding factor 2 (Nrbf2) as a Beclin 1-interacting protein from *Becn1*^{-/-};*Becn1-EGFP*/+ mouse liver and brain. We also found that Nrbf2-Beclin 1 interaction required the N-terminus of Nrbf2. We next used human retinal pigment epithelial cell line RPE-1 as a model system and showed that transiently knocking down Nrbf2 by siRNA increased autophagic flux under both nutrient-rich and starvation conditions. To investigate the mechanism by which Nrbf2 regulates autophagy, we demonstrated that Nrbf2 interacted and colocalized with Atg14L, suggesting that Nrbf2 is a component of the Atg14L-containing Beclin 1-Vps34 complex. Moreover, ectopically expressed Nrbf2 formed cytosolic puncta that were positive for isolation membrane markers. These results suggest that Nrbf2 is involved in autophagosome biogenesis. Furthermore, we showed that Nrbf2 deficiency led to increased intracellular phosphatidylinositol-3 phosphate levels as well as diminished Atg14L-Vps34/Vps15 interactions, suggesting that Nrbf2-mediated Atg14L-Vps34/Vps15 interactions likely inhibit Vps34 activity. Therefore, we propose that Nrbf2 may interact with the Atg14L-containing Beclin 1-Vps34 protein complex to modulate protein-protein interactions within the network, leading to suppression of Vps34 activity, autophagosome biogenesis and autophagic flux. This work reveals a novel aspect of the intricate mechanism for the

Beclin 1-Vps34 protein-protein interaction network to achieve precise control of autophagy.

Introduction

Autophagy is an essential lysosomal degradation pathway that eukaryotic cells employ to recycle cytoplasmic contents for providing building blocks and energy. Macroautophagy, the primary form of autophagy and referred to as autophagy hereafter, is characterized by (i) sequestration of the bulk of the protein- and organelle-containing cytoplasm into *de novo* generated double-membraned structures called autophagosomes (autophagosome biogenesis), and (ii) subsequent fusion of autophagosomes with late endosomes or lysosomes for degradation of the enwrapped cytoplasmic contents (autophagosome maturation) (1). Whereas autophagy deficiency has been implicated in a broad spectrum of human diseases including liver diseases, cardiovascular diseases, cancer, and neurodegeneration (2), hyperactive autophagy may lead to cell death (*e.g.*, autosis (3)). Therefore, autophagy must be tightly regulated for fitness and survival.

Becn1, the ortholog of yeast *Vps30/Atg6* gene, is one of the first discovered mammalian autophagy genes (4). Beclin 1, encoded by *Becn1*, was originally reported as a Bcl-2 interacting protein through a yeast two-hybrid screen of an adult mouse brain cDNA library (5,6). Beclin 1/Vps30 plays important roles in autophagy regulation, likely through its numerous interacting proteins. In yeast, Vps30 forms two distinct protein complexes with Vps34, the only known class III phosphatidylinositol 3-kinase that catalyzes the conversion of phosphatidylinositol (PtdIns) to phosphatidylinositol 3-phosphate (PI3P) (7,8). One Vps30-Vps34 complex is recruited to the pre-autophagosomal structure (PAS) by Atg14 (9) and functions to produce PI3P during autophagosome biogenesis. The other Vps30-Vps34 complex contains Vps38 and is involved in the vacuolar protein sorting (Vps) pathway (10). Likewise, in mammals, Beclin 1 and its interactors form multiple protein complexes for diverse functions (comprehensively reviewed in (11-13)). Some of the Beclin 1-interacting proteins, *e.g.*, Vps34 (14), Atg14L (15,16) (also named Atg14 (17) and Barkor (18)), p110 β (19), Ambra1 (20), VMP1 (21,22), and HGMB1 (23), positively regulate autophagy. Others, *e.g.*, Rubicon (15,16) and Bcl-2/X_L (24), are negative regulators of autophagy. In particular, Beclin 1 also forms two major protein complexes with

Vps34: One is the Atg14L-containing Beclin 1-Vps34 protein complex that is involved in autophagosome biogenesis (15-18,25,26); the other is the UVRAG-containing Beclin 1-Vps34 protein complex that is involved in endocytic trafficking (17,27) and, with some controversy, in autophagy regulation (17,28). In short, based on extensive investigation reviewed above, a theme has emerged for the presence of a central autophagy regulation hub composed of a dynamic Beclin 1-Vps34 protein-protein interaction network.

Despite the importance of the Beclin 1-Vps34 protein-protein interaction network in regulating autophagy and for tumor suppression (4,28-32), development (20,30,33), aging (34,35), and neurodegeneration (36,37), the molecular details of how this network regulates autophagy are not fully understood. In this work, we set out to determine additional key players in the Beclin 1-Vps34 protein-protein interaction network and identified nuclear receptor binding factor 2 (Nrbf2) as a Beclin 1-interacting protein. Nrbf2 was originally reported to interact with nuclear receptors as a co-regulator (38,39). Here, we determined a novel role for Nrbf2 in autophagy regulation through modulating the Beclin 1-Vps34 protein-protein interaction network.

Experimental procedures

A. Reagents and antibodies

NuPAGE® Bis-Tris gels, Western blot transfer buffer, MOP and MES SDS running buffers, NuPAGE® antioxidant, glutamine (25030), fetal bovine serum (FBS) (Gibco 26140), SlowFade® Gold antifade reagent (S36937), Opti-MEM® I Reduced Serum Medium (31985), Ambion® Micropoly (A)Purist™ Kit (AM1919), SuperScript™ III First-Strand Synthesize System for RT-PCR (18080-051), SYBR® safe DNA gel stain (S33102), pENTR™ Directional TOPO® Cloning Kit (K2400-20), TOPO® TA Cloning Kit (K450001), Lipofectamine 2000 (11668), Lipofectamine RNAi MAX (13778), and ProLong® Gold antifade reagent (P36934) were purchased from Invitrogen (Carlsbad, CA). Restriction enzymes and Quick Ligation Kit (M2200S) were purchased from New England BioLabs (Ipswich, MA). TaKaRa LA PCR Kit 2.1 (#RR013A) and pmCherry-C1 vector (632524) were purchased from Clontech (Mountain View, CA). Wizard® Plus SV Minipreps DNA

Purification System (A1330) was purchased from Promega (Madison, WI). Plasmid Plus Maxi Kit (12963) and RNeasy Mini Kit (74014) were purchased from QIAGEN (Valencia, CA). The iScript™ cDNA Synthesis Kit (170-8890) and SsoAdvanced™ Universal SYBR® Green Supermix (172-5271) were purchased from Bio-Rad Laboratories, Inc. (Richmond, CA). Bafilomycin A1 (Baf) from *Streptomyces griseus* (B1793), trichloroacetic acid (TCA) (T6399), BSA (A7906) and the trypsin-EDTA solution (T4049) were purchased from Sigma (St. Louis, MO). EDTA-free protease inhibitor cocktail tablets (11836170001) and PhosSTOP phosphatase inhibitor cocktail tablets (04906837001) were purchased from Roche Diagnostics (Indianapolis, IN). Pierce Halt Protease and Phosphatase Inhibitor Cocktail (78443), Subcellular Protein Fractionation Kit (78840), SuperSignal West Pico Chemiluminescent Substrate (34080), SuperSignal West Femto Maximum Substrate (34096), Micro BCA Protein Assay Reagent Kit (23235), and Dharmacon siRNAs were purchased from Thermo Scientific (Rockford, IL). Immobilon-P 0.2 µm PVDF membrane (ISEQ00010) and 10× RIPA lysis buffer (20-188) were purchased from Millipore (Billerica, MA). PI(3)P Mass Strip™ Kit (K-3600) and PI(3)P Mass ELISA Kit (K-3300) were purchased from Echelon Biosciences (Salt Lake City, UT). Dulbecco's Modification of Eagle's Medium (DMEM, Cellgro 10-013-CV) was purchased from Corning (Manassas, VA). L-leucine (L2020-05) and DMEM high glucose with pyridoxal•HCl without L-glutamine and leucine (D9816) were purchased from USBiological (Marblehead, MA). Econo-Safe Economical Biodegradable Counting Cocktail (111175) was purchased from Research Products International Corporation (Mount Prospect, IL). Four-well slides coated with type I collagen (354557) were purchased from BD Biosciences (Franklin Lakes, NJ). Recombinant protein A beads (IPA-300) was purchased from Repligen (Waltham, MA).

For Western blotting, Beclin 1 (H300) antibody (sc-11427, 1:500), Ulk1 (H-240) antibody (sc-33182, 1:500), anti-rabbit IgG-HRP (sc-2004) and anti-mouse IgG-HRP (sc-2005) antibodies were purchased from Santa Cruz Biotechnology (Santa Cruz, CA). Nrbf2 antibody (A301-852A, 1:5000) and Vps15/p150 (A302-571A, 1:4000) were purchased from Bethyl Laboratories (Montgomery, TX). Guinea pig anti-p62 antibody (03-GP62-C, 1:1700) was purchased

from ARP American Research Products (Waltham, MA). Anti-LC3 (clone 2G6) antibody (0260-100, 1:1000) was purchased from nanoTools Antikörpertechnik GmbH & Co. KG (Teningen, Germany). Phospho-p70 S6 kinase (Thr 389) antibody (9205, 1:1000), p70 S6 kinase antibody (clone 49D7) (2708, 1:1000), Vps34 antibody (clone D9A5) (4263, 1:1000) and Atg14L antibody (5504, 1:1000) were purchased from Cell Signaling (Danvers, MA). Peroxidase-rabbit anti-Guinea Pig IgG (H+L) was purchased from Invitrogen (Carlsbad, CA). Anti- β -actin (clone AC-15) mouse monoclonal antibody (A5441, 1:10000) was purchased from Sigma (St. Louis, MO).

For immunoprecipitation (IP), Atg14L (PD026) and UVRAG (M160-3) antibodies were purchased from MBL International (Woburn, MA). Vps34 antibody (Z-R015) was purchased from Echelon Biosciences (Salt Lake City, UT). Beclin 1 antibody (A302-567A) was purchased from Bethyl Laboratories (Montgomery, TX). For immunofluorescent imaging, c-myc antibody (9E10) (sc-40, 1:1000) was purchased from Santa Cruz Biotechnology (Santa Cruz, CA) and FIP200 antibody (10043-2-AP, 1:400) was purchased from ProteinTech Group, Inc (Chicago, IL). Rhodamine RedTM-X Goat Anti-Mouse IgG (H+L) (R-6393) and Alexa Fluor[®] 488 Goat Anti-Rabbit IgG (H+L) Antibody (A11034) were purchased from Invitrogen (Carlsbad, CA).

B. Plasmid construction

Total mRNA was isolated from HepG2 cells and purified using the Micropoly (A)PuristTM Kit. Human Nrbf2 (Ensembl transcript ID: ENST00000277746) cDNA was PCR-amplified using SuperScriptTM III First-Strand Synthesize System. Full length Nrbf2 inserts intended for N- and C-terminal tagging were generated by N- and C-terminal specific primers, respectively. For N-terminal tagging, the forward primer was 5' CAC CCA AAT GGA AGT AAT GGA AGG AC 3'; and the reverse primer was 5' CTA ATT ATT CAT AAA TCC TTT CAG AAT 3'. For C-terminal tagging, the forward primer (#5) was 5' CAC CAT GGA AGT AAT GGA AGG ACC CC 3'; and the reverse primer (#8) was 5' ATT ATT CAT AAA TCC TTT CAG AAT AT 3'. To generate the C-terminal tagged Nrbf2 truncation mutants M1-M6, the reverse primers for M1 was 5' CTG CTC TGA CTG TGT CAG CTT CAT GGC TT 3'; the forward primer for M2 was 5' CAC CAT GGC CAT GAA GCT GAC ACA

GTC AGA 3'; the reverse primer for M3 was 5' GCT GTA CTT CTG AGA AAG GGG ACT CTG 3'; the forward primer for M4 was 5' CAC CAT GGC TCC TTC CAC AGA GAA ATG CCT G 3'; the reverse primer for M5 was 5' ATC AGC ATC TAC ATC CAG CTC CTT TTC 3'; and the reverse primer for M6 was 5' GGC TTT GCT TCC AAT ACA TGG CTC TGC T 3'. These primers were used in combination with primers #5 and #8. Inserts containing the cDNAs of full length Nrbf2 and the truncation mutants were originally inserted into Gateway pENTRTM/D-TOPO entry vector and correctness of the insertions was confirmed by sequencing. C-terminal cycle 3 GFP-tagged full length Nrbf2 and the truncation mutants were generated using the Gateway destination vector pcDNATM-DEST47. Full length Nrbf2 cDNA in the Gateway entry vector was amplified using TaKaRa LA PCR Kit 2.1 as well as forward primer 5' CCG GCT AGA TCT ATG GAA GTA ATG GAA GGA CCC 3' and reverse primer 5' CCG GCT GTC GAC TTA ATT ATT CAT AAA TCC TT 3'. Nrbf2 amplicon was later sub-cloned into pCR2.1-TOPO vector, excised using restriction enzymes BglII and Sall, and cloned into mCherry-C1 vector using New England BioLabs Quick Ligation Kit. All positive clones were verified by restriction digest and sequencing. All oligonucleotides were synthesized by Integrated DNA Technologies. For cloning, all plasmid DNAs were prepared using E. coli DH5 α or TOP10 cells and the Promega Wizard[®] Plus SV Minipreps DNA Purification System. For transfection into mammalian cells, all plasmids were prepared using the QIAGEN Plasmid Plus Maxi Kit.

C. Cell culture and biochemical analyses

Unless otherwise noted, RPE-1 cells were cultured in DMEM supplemented with 10% FBS, 100 U/ml penicillin, and 100 μ g/ml streptomycin in a cell culture incubator (set at 37°C and 5% CO₂). For overexpression, cells at 70-80% confluency in 6-cm dishes were transfected with 4 μ g of mCherry C1 vector or human mCherry-Nrbf2 plasmid using Opti-MEM[®] I Reduced Serum Medium and Lipofectamine 2000, following manufacturer's instructions. Twenty-four hours after transfection, cells were washed with PBS and cultured in either nutrient-rich or starvation (*i.e.*, 18 h serum starvation or 1 h Hank's buffer starvation) conditions in the presence or absence of 200 nM Baf for 18 h. Different cells showed different sensitivities in

response to Baf. We chose to treat RPE-1 cells with 200 nM Baf for 18 h in this study, because in our hands, this treatment resulted in prominent changes in LC3II levels in RPE-1 cells whereas 2 h 100 nM Baf treatment had minimal effect.

For siRNA treatments, cells were reversely transfected with 20 nM of each siRNA using Opti-MEM® I Reduced Serum Medium and Lipofectamine RNAiMAX, following manufacturer's instructions. In brief, $6-8 \times 10^5$ cells were suspended to 3 ml of DMEM medium supplemented with 10% FBS without antibiotics. siRNAs were added to the cell suspensions to a final concentration of 20 nM each. These siRNAs were Dharmacon ON-TARGETplus non-targeting siRNA pool (D-001810-10-20) and smartpool siRNA targeting human Nrbf2 (L-014648-00-0005), Atg14L (L-020438-01-0005), Beclin 1 (L-010552-00-0005), and Vps34 (L-005250-00-0005). The sequence of the human UVRAG siRNA is 5' UCA CUU GUG UAG UAC UGA AUU 3', with the target sequence (28) underscored. The sequence of the human Nrbf2 3'UTR siRNA is 5' UGU GAA AUG CGC UGC GUA UUU 3', with the target sequence underscored. The cell-siRNA mixtures were seeded onto 6-cm dishes. Cells were cultured for 48-72 h before subject to either nutrient-rich or starvation conditions in the presence or absence of 200 nM Baf for 18 h.

To harvest cells for biochemical analysis, cell monolayers were washed with ice-cold PBS and collected on ice using scrapers. Cell pellets were lysed on ice with 1x RIPA lysis buffer supplemented with protease and phosphatase inhibitor cocktail using 1 ml syringe and 27G1/2 needles. Cell lysates were centrifuged at $14,000 \times g$ and $4^\circ C$ for 5 min and supernatant was used for Western blot analyses on an equal protein basis (15-40 μg). For resolving LC3I and LC3II, cell lysates were run on 10% or 12% Bis-Tris gels using MOP or MES buffer. For probing all other proteins, cell lysates were run on 4-12% Bis-Tris gels using MOP buffer. Proteins were transferred to PVDF membranes using a Mini Trans-Blot apparatus (Bio-Rad) at 30 V overnight in Western blot transfer buffer (Invitrogen) supplemented with NuPAGE® antioxidant, 20% methanol, and 0.025% SDS. Membranes were then incubated with primary and secondary antibodies, and signals were detected by SuperSignal West Pico/Femto Chemiluminescent Substrate. Films were exposed for various time periods and

scanned using positive mode to ensure that data were obtained within a linear range of exposure. The p62 (or LC3II) levels were quantified using ImageJ and normalized to corresponding actin levels. The p62 (or LC3II)/actin ratios were further normalized to the samples with mCherry empty vector or Ctl siRNA treatments. Comparisons were made in Excel using a one-sample two-tailed student's t-test. For subcellular fractionation, harvested cell pellets were processed using Pierce Subcellular Protein Fractionation Kit, following manufacturer's instructions.

IP was carried out as reported (40). In brief, RPE-1 cells grown in 10-cm dishes were transfected with different siRNA as described above. After 48 h, cells were lysed with 1 ml of Mild Lysis Buffer (MLB, 10 mM Tris, PH7.5, 2 mM EDTA, 100 mM NaCl, 1% NP-40, 50 mM NaF, 1 mM Na_3VO_4 , EDTA-free protease inhibitor cocktail (Roche) and Pierce Halt Protease and Phosphatase Inhibitor Cocktail. Cell lysates, except for 100 μl aliquots saved for probing INPUT, were used for IP. Anti-Beclin 1, anti-Nrbf2, anti-Atg14 and anti-Vps34 antibodies were coupled with Repligen Immobilized Protein A-agarose beads overnight at $4^\circ C$ in TBST (20 mM Tris, pH.8.0, 170 mM NaCl, and 0.05% Tween-20) supplemented with 1% BSA. The immune complex was then added to cell lysates and incubated at $4^\circ C$ for 3 h. The resulting beads were washed with MLB five times before the antigen and their interacting proteins were eluted by SDS-PAGE loading buffer.

D. Long-lived protein degradation

Long-lived protein degradation was measured following a published protocol (41) with minor modifications. In brief, RPE-1 cells were reversely transfected with 20 nM of non-targeting siRNA, human Nrbf2 and Atg14L smartpool siRNA using Opti-MEM® I Reduced Serum Medium and Lipofectamine RNAiMAX in either hot or cold media. Hot medium was composed of L-glutamine- and leucine-free DMEM supplemented with 10% FBS, 4 mM L-glutamine, 65 μM of cold L-leucine and 1 $\mu Ci/ml$ 3H -L-leucine. Cold medium had all compositions of the hot medium except for hot L-leucine. After being pulse-labeled for 24 h, cells were washed twice with sterile PBS (at room temperature) and cultured in cold medium for 20 h to chase out short-lived proteins. Cells were then washed twice with sterile PBS (at room temperature) and cultured in 2 ml cold medium either without or

with 10% FBS for 8 h to degrade long-lived proteins. Long-lived protein degradation was calculated from the TCA-soluble radioactivity of the media and the TCA-precipitated radioactivity of the cell monolayers. A volume of 860 μ l of medium was taken from each plate and mixed thoroughly with 140 μ l of 71.4% TCA (final TCA concentration 10%). The mixtures were incubated on ice for 1 h before centrifuged at 17,720 \times g for 10 min at 4°C. An aliquot of 0.4 ml of the supernatant was mixed with 4 ml of scintillation counting cocktail for measuring the content of tritium in the medium using a scintillation counter. The total counts in the supernatant were labeled as A. The cell monolayers were washed with ice-cold PBS once. Cells were fixed to the plate by 2 ml ice-cold 10% TCA for 40 min at 4°C. The cell monolayers were washed with 2 ml ice-cold 10% TCA once, lysed in 2 ml of 0.2 M NaOH (pre-warmed to 37°C), and incubated at 37°C for 1 h. An aliquot of 0.4 ml of the lysate was used to measure tritium content in the cell monolayer. The total counts in the pellet were labeled as B. The average rate of long-lived protein degradation during the 8 h for degrading long-lived proteins was calculated as $A/(A+B)$. Data from three independent experiments were averaged, with each experiment having triplicated samples. Comparisons were made using ANOVA.

E. Fluorescence microscopy

RPE-1 cells were seeded in type I collagen-coated 4-well slides at a density of 5×10^4 cells per well. For transient expression, cells were transfected with a total of 1 μ g plasmid(s) in each well using Lipofectamine 2000 and Opti-MEM® I Reduced Serum Medium 24 h after being seeded. Twenty-four after transfection of plasmid(s), cells were washed once with Hank's buffer and cultured in Hank's buffer at 37°C in the presence of 5% CO₂ for 1 h. Afterwards, cells were fixed in 4% paraformaldehyde in PBS for 15 min, permeabilized with 50 μ g/ml digitonin for 10 min, and blocked with 2% goat serum and 2% BSA in PBS for 30 min at room temperature. Cells were then incubated in primary antibodies against c-myc and FIP200, respectively, overnight at 4°C, followed by dye conjugated secondary antibodies for 1 h at room temperature. After four washes, liquid in wells was aspirated before the slides were mounted with ProLong® Gold antifade reagent and 1.5 mm-thick cover glass. Confocal fluorescent images were collected on a Nikon A1 confocal microscope equipped with an Apo TIRF

60 \times oil objective lens (numerical aperture 1.49) and quantified manually using the Nikon NIS-Elements AR 3.2 software. Cells with low-to-medium expression levels and with best morphology were imaged. Image intensity levels were processed linearly to enhance contrast. Comparisons were made in Excel using a two-sample two-tailed student's t-test.

F. Protein-lipid overlay and ELISA assays

Extraction and detection of total intracellular PI3P were carried out using a PI(3)P Mass Strip Kit and a PI(3)P Mass ELISA Kit, following manufacturer's instructions. Briefly, cells were first fixed with 0.5 M ice-cold TCA on ice for 5 min. Next, fixed cells were harvested on ice using scrapers. Cell suspension was centrifuged at 1,500 rpm for 5 min at 4°C and cell pellets were washed twice with 5% TCA in the presence of 1 mM EDTA. Neutral lipids were extracted with Methanol (MeOH): Chloroform (CHCl₃) (2:1) for 10 min at room temperature with three times of vortexing during the extraction. After centrifugation at 1,500 rpm for 5 min at 4°C, supernatant containing neutral lipids was discarded. Extraction and removal of neutral lipids were repeated once. Acidic lipids including PI3P were then extracted by CHCl₃: MeOH: 12M HCl (40:80:1) for 15 min at room temperature with four times of vortexing during the extraction. After centrifugation at 1,500 rpm for 5 min at 4°C, supernatant containing acidic lipids was transferred to new tubes. CHCl₃ and 0.1 M HCl were added sequentially to the supernatant. The tubes were vortexed and then centrifuged at 1,500 rpm for 5 min at 4°C. Organic (lower) phase containing acidic lipids was transferred to new tubes and dried in a vacuum dryer. Cell pellets were lysed by incubation in 0.1 M NaOH overnight at a 37 °C shaker. The protein concentrations of lysates were measured by a Micro BCA Protein Assay Reagent Kit following manufacturer's instructions.

To carry out the protein-lipid overlay assay, dried acidic lipids were reconstituted with 10 μ l of CHCl₃: MeOH: H₂O (1: 2: 0.8). The samples were vortexed and sonicated in icy water bath. Lipid solutions were spotted onto PI3P strips and dried at room temperature. The strips were blocked with 3% BSA, and then incubated with 5 μ g of PI3P-binding protein. The PI3P spots were detected with SuperSignal West Femto Maximum Substrate. Intracellular PI3P levels were quantified using ImageJ and normalized to total protein

levels. Comparisons were made in Excel using two-sample one-tailed student's t-test.

To measure total intracellular PI3P by the quantitative and competitive ELISA assay, dried acidic lipids were reconstituted in PBST (PBS and 0.05% Tween-20) with 3% Protein Stabilizer. Reconstituted samples were incubated with PI3P detector protein before transferred to a microplate pre-coated with PI3P for competitive binding. A peroxidase-conjugated antibody against PI3P detector protein was added and colorimetric detection was carried out to determine PI3P detector protein binding on the microplate. Total intracellular PI3P quantities were calculated using the standard curve from logarithmic fitting of manufacturer-supplied PI3P standards, and normalized to total protein levels. Comparisons were made in Excel using one-tailed paired student's t-test.

G. Sequence alignment

Sequence alignment was carried out in the Biology Workbench (<http://workbench.sdsc.edu/>) using CLUSTALW and CLUSTALWPROF with default settings. The results were displayed using TEXSHADE.

H. Quantitative reserve transcription (qRT)-PCR

RPE-1 cells that were reserve-transfected with non-targeting, smartpool and 3'UTR *Nrbf2* siRNA were seeded into 60 mm dishes and cultured for 48 h before total mRNA was extracted using the Qiagen RNeasy Mini Kit, following the manufacturer's instructions. Purified mRNA (1 µg) from each sample was converted to cDNA in 20 µl reaction mixtures using the iScript™ cDNA Synthesis Kit, following the manufacturer's protocols. Subsequent qRT-PCR of target transcripts were performed in 20 µl reaction mixtures each composed of 2 µl (20 ng) of cDNA, 10 µl of SsoAdvanced™ Universal SYBR® Green Supermix, 1-2 µl qRT-PCR primer probe set, and 6-7 µl nuclease-free water. The qRT-PCR primers used for human *p62/SQSTM1* transcript (Hs.PT.56a.40413286.g; forward primer 5' GGA GGA GAT GAT GAC TGG AC 3'; reverse primer 5' CAG AGA GCT TGG CCC TTC 3') and the control human *ACTB* transcript (Hs.PT.56a.19461448.g; forward primer 5' GCG AGA AGA TGA CCC AGA T 3'; reverse primer 5' CCA GTG GTA CGG CCA GA 3') were purchased from Integrated DNA Technologies. Forty cycles of amplification were performed in a Stratagene Mx3005P QPCR system (Agilent

Technologies), according to the manufacture's specifications. Three replicates were performed for each probe-cDNA combination. The fold change of human *p62/SQSTM1* transcript in response to the smartpool or 3'UTR *Nrbf2* siRNA treatment was calculated from the cycle number at the threshold SYBR® Green signal (Ct) as follows:

$$p62 \text{ transcript fold change} = \frac{2^{(Ct_{non-targeting\ siRNA,p62} - Ct_{Nrbf2\ siRNA,p62})}}{2^{(Ct_{non-targeting\ siRNA,ACTB} - Ct_{Nrbf2\ siRNA,ACTB})}}$$

Note that in this equation, *ACTB* was used as the control to account for the variations in the total mRNA quantity.

Results

A. Identification of *Nrbf2* as a Beclin 1-interacting protein

Utilizing the Bacterial Artificial Chromosome (BAC) technique, we previously generated compound mouse *Becn1-EGFP/+;Becn1^{-/-}*, which expressed Beclin 1-EGFP under the endogenous *Becn1* promoter and in the genetic background of the homozygous Beclin 1 knockout mouse *Becn1^{-/-}* (15). Remarkably, Beclin 1-EGFP rescued embryonic lethality of *Becn1^{-/-}*, suggesting that the transgene is functional in the compound mouse (15). We previously also affinity purified and mass spectrometrically identified a number of Beclin 1-interacting proteins from the brain and liver of the rescued mice, including Vps34, Vps15, UVRAG, Atg14L, and Rubicon (**Figure 1b** in (15)). One additional Beclin 1-interacting protein with an apparent mass of 38 kDa was identified as *Nrbf2* (mass spectra not shown). Here, using an anti-GFP antibody to perform reciprocal IP in HEK 293 cells stably expressing *Nrbf2-EGFP*, we showed that *Nrbf2-EGFP* was capable of pulling down endogenous Beclin 1 and Vps34 under both nutrient-rich and serum-starvation conditions (**Figure 1a**), confirming the *Nrbf2-Beclin 1* interaction. Moreover, to assess endogenous interactions between *Nrbf2* and some known Beclin 1-Vps34 complex components, we used an anti-*Nrbf2* antibody to perform IP from the retinal pigment epithelium cell line RPE-1 cultured under nutrient-rich conditions. Our result shows that anti-*Nrbf2* antibody was capable of pulling down endogenous Beclin 1, Vps34 and Vps15 from RPE-1 cells transfected with non-targeting siRNA, but not from RPE-1 cells transfected with *Nrbf2* siRNA (**Figure 1b**). This result further shows that at endogenous levels, *Nrbf2* interacts with the core

of the Beclin 1-Vps34 protein-protein interaction network. Nrbf2-Beclin 1 interaction was also independently discovered by Harper's group in a large-scale proteomic study of the human autophagy network (42). Taken together, our results demonstrate that Nrbf2 is a component of the Beclin 1-Vps34 protein-protein interaction network.

Human Nrbf2 protein is 287 amino-acid long. It has an N-terminal Microtubule Interacting and Trafficking domain (MIT, amino acids 8-52) that has been reported in vacuolar sorting proteins and a C-terminal Domain of Unknown Function (DUF1875, amino acids 45-287) which contains a Coiled-Coil Domain (CCD, amino acids 167-215) for protein-protein interactions (**Figure 1c-d**). To determine which domain of Nrbf2 interacts with Beclin 1, we generated C-terminal GFP-tagged full length and truncation mutants of Nrbf2 (**Figure 1c**). We transiently transfected HepG2 cells with these constructs and performed anti-GFP IP from cell extracts. Our result shows that full length Nrbf2 and truncation mutants M3 (amino acids 1-120), M5 (amino acids 1-220) and M6 (amino acids 1-160) pulled down endogenous Beclin 1; in contrast, truncation mutants M1 (amino acids 1-52), M2 (amino acids 45-287) and M4 (amino acids 120-287) were largely unable to pull down endogenous Beclin 1, suggesting that the N-terminus of Nrbf2 (*i.e.*, amino acids 1-120) is important for Nrbf2-Beclin 1 interaction (**Figure 1e**, short exposure). To detect any trace of M1/M2/M4 mutant Nrbf2-Beclin 1 interaction, we exposed the film for a longer time and found that small amount of endogenous Beclin 1 was pulled down by the truncation mutants M2 and M4, but not M1 (**Figure 1e**, long exposure). Interestingly, truncation mutants M2, M4, and M5, all of which contain the CCD, pulled down endogenous Nrbf2, suggesting that Nrbf2 is likely capable of self-association through its CCD (**Figure 1e**). Therefore, our observation that small amount of endogenous Beclin 1 was pulled down by M2 and M4 was likely resulted from the CCD-mediated interactions between the truncation mutant M2/M4 and the full-length Nrbf2. Taken together, our results suggest that the N-terminus of Nrbf2 (*i.e.*, amino acids 1-120, including both the MIT domain and the amino acids 53-120) is necessary and sufficient for the Nrbf2- Beclin 1 interaction.

B. Nrbf2 negatively regulates autophagic flux

Because the Beclin 1-Vps34 protein-protein interaction network is a key regulatory hub

for autophagy, we next assessed the role of Nrbf2 on autophagic activity. To do that, we carried out three widely-used autophagic flux assays. The first involves measuring the steady state levels of p62/SQSTM1 protein, an adaptor for delivering autophagy substrates to autophagosomes while the adaptor itself is degraded along with the substrates in autolysosomes (43). We treated RPE-1 cells with non-targeting (labeled Ctl for control) siRNA, a pool of four siRNAs against the open reading frames (ORFs) of human Nrbf2 (labeled sp for smartpool), or a single siRNA against the 3' untranslated region of human Nrbf2 (labeled 3'UTR). Our data show that treating cells with either the smartpool or the 3'UTR Nrbf2 siRNA, as compared to non-targeting siRNA, decreased p62 protein levels under both nutrient-rich and Hank's buffer starvation conditions (**Figure 2a**). We further examined if decreased p62 protein levels upon Nrbf2 siRNA treatments were resulted from reduced p62 transcript levels. To do that, we performed RNA-Seq analysis of RPE-1 cells treated with non-targeting, smartpool and 3'UTR Nrbf2 siRNAs. We found that p62 transcripts were highly abundant in RPE-1 cells and not significant changed upon Nrbf2 siRNA treatments (data not shown). We also performed qRT-PCR analysis of RPE-1 cells treated with non-targeting, smartpool and 3'UTR Nrbf2 siRNAs. We confirmed that p62 transcripts in RPE-1 cells were not significant changed upon Nrbf2 siRNA treatments (**Figure 2b**). Therefore, the reduction in the p62 protein levels in the Nrbf2-deficient RPE-1 cells was likely a result of an increased autophagic flux. We also observed similar decrease of p62 protein levels in the HepG2 cells treated with either smartpool or 3'UTR Nrbf2 siRNA, as compared to non-targeting siRNA (**Figure 2b**), suggesting that the increase of autophagic flux in response to Nrbf2 deficiency is likely a common phenomenon for human cells. Therefore, in the rest of the study, we focused on RPE-1 cells. Of note, while the smartpool Nrbf2 siRNA depleted Nrbf2 protein more effectively than the 3'UTR Nrbf2 siRNA in both RPE-1 and HepG2 cells, the 3'UTR Nrbf2 siRNA reduced p62 protein levels more effectively than the smartpool Nrbf2 siRNA (**Figure 2a,c**). It is possible that either 3'UTR Nrbf2 siRNA has an off-target effect which increases p62 degradation by the ubiquitin proteasome system or the smartpool Nrbf2 siRNA has an off-target effect which decreases p62 degradation by the ubiquitin proteasome system. We have no data to favor one

over the other. Therefore, we chose to use the smartpool Nrbf2 siRNAs hereafter, solely based on knockdown efficiency. In addition, Nrbf2 siRNA (as compared to non-targeting siRNA) decreased p62 protein levels under serum starvation conditions, similar to the observation under either nutrient-rich or Hank's buffer starvation conditions (**Figure 2d**), suggesting that increase of autophagic flux in response to Nrbf2 deficiency is likely a common phenomenon for different nutrient conditions. Therefore, in the rest of the study, we used either Hank's buffer starvation or serum starvation.

The second autophagic flux assay involves monitoring the changes in the levels of LC3II in response to lysosomal inhibitors (*e.g.*, Bafilomycin A1 (Baf), an inhibitor of the vacuolar H⁺-ATPase and thus lysosomal acidification and autophagosome-lysosome fusion (44)) (45,46). Using this assay, we observed that under both nutrient-rich and serum-starvation conditions, transfecting Nrbf2 siRNA (as compared to non-targeting siRNA) led to a greater increase in the LC3II levels in response to Baf, suggesting that Nrbf2 deficiency increases autophagic flux (**Figure 2e**). Conversely, overexpressing mCherry-tagged Nrbf2 (as compared to mCherry empty vector) led to a smaller increase in the LC3II levels upon Baf treatment, suggesting that Nrbf2 overexpression decreases autophagic flux (**Figure 2f**).

The third autophagic flux assay directly measures the rate of long-lived protein degradation by pulse-chasing with a radioactively labeled amino acid (*e.g.*, ¹⁴C-Leu). Our data show that as compared to non-targeting siRNA, Nrbf2 siRNA treatment increased long-lived protein degradation under both nutrient-rich and serum-starvation conditions (**Figure 2g**). Collectively, these autophagic flux data suggest that Nrbf2 negatively regulates basal and starvation-induced autophagy.

C. Nrbf2 is a component of the Atg14L-containing Beclin 1-Vps34 protein complex

Because we identified Nrbf2 as a Beclin 1-interacting protein and because it is well known that there are at least two Beclin 1-Vps34 protein complexes, we asked which Beclin 1-Vps34 protein complex Nrbf2 was associated with. The two main Beclin 1-Vps34 protein complexes contain exclusively Atg14L or UVRAG, with the Atg14L-containing complex known to be involved in autophagosome biogenesis (15-18,25,26). We first tested if Nrbf2 was associated with the

Atg14L-containing Beclin 1-Vps34 protein complex. To do that, we transiently transfected cells with EGFP-tagged full length Atg14L or mutant Atg14L with either the first or both of the CCDs deleted (labeled Δ CCD1 and Δ CCD1 Δ CCD2, respectively) (15) and performed anti-GFP IP. Our data show that EGFP-tagged full length Atg14L, but not the Δ CCD1 or Δ CCD1 Δ CCD2 mutant of Atg14L, pulled down endogenous Nrbf2 (**Figure 3a**), suggesting that Nrbf2 interacts with Atg14L in an Atg14L CCD-dependent manner.

We then tested if Nrbf2 and Atg14L colocalized. Our data show that ectopically expressed mCherry-Nrbf2 and Atg14L-EGFP largely colocalized on punctate structures in RPE-1 cells under both nutrient-rich and serum starvation conditions (**Figure 3b** arrows and quantified in **Figure 3c**). This result is consistent with the presence of the Nrbf2-Atg14L interaction.

To dissecting the role of the Nrbf2-Atg14L interaction, we performed anti-Beclin 1 IP from RPE-1 cells treated with non-targeting, Nrbf2, Atg14L, or UVRAG siRNA. Our data show that Atg14L, but not UVRAG, was required for the Beclin 1-Nrbf2 interaction (**Figure 3d, lanes 7-8**); in contrast, Nrbf2 was not required for the interaction of Beclin 1 with Atg14L, UVRAG, Vps34, or Vps15 (**Figure 3d, lane 6**). We further performed anti-Nrbf2 IP from RPE-1 cells treated with non-targeting, Nrbf2, Atg14L or Vps34 siRNA. Our data show that Nrbf2 pulled down not only Beclin 1, Vps34, and Vps15, but also Atg14L; however, Nrbf2 was unable to pull down UVRAG (**Figure 3e, lane 5**). Our data also show that anti-Nrbf2 IP from RPE-1 cells treated with Atg14L siRNA was unable to pull down Beclin 1 even though Beclin 1 was reasonably stable in the absence of Atg14L, confirming the requirement of Atg14L for the Beclin 1-Nrbf2 interaction (**Figure 3e, lanes 3 & 7**). In addition, anti-Nrbf2 IP from RPE-1 cells treated with Atg14L siRNA was also unable to pull down Vps15 and only capable of pulling down a small fraction of Vps34, even though both Vps34 and Vps15 were stable in the absence of Atg14L (**Figure 3e, lanes 3 & 7**). These results suggest that association of Nrbf2 with the Beclin 1-Vps34 protein complex is primarily mediated by Atg14L, and Nrbf2 is largely associated with the Atg14L-containing, rather than the UVRAG-containing, Beclin 1-Vps34 protein complex.

We previously reported that ectopically co-expressed Beclin 1 and Atg14L colocalized on cytosolic punctate structures that were enwrapped with double-membranes and contained electron-dense materials, consistent with a role for the Atg14L-containing Beclin 1-Vps34 protein complex in autophagosome biogenesis (15). Here we further showed that in RPE-1 cells transiently co-transfecting with Nrbf2-EGFP, FLAG-Beclin 1 and Atg14L-AsRed, Nrbf2-EGFP localized on the FLAG-Beclin 1- and Atg14L-AsRed-positive cytosolic puncta known to be wrapped by double membranes (**Figure 3f**). Therefore, our data collectively suggest that Nrbf2 is primarily associated with the Atg14L-containing Beclin 1-Vps34 protein complex that is known to participate in autophagosome biogenesis.

D. Nrbf2 is involved in autophagosome biogenesis

We therefore directly examined if Nrbf2 was involved in autophagosome biogenesis. Using subcellular fractionation, we first showed that in the HEK293 cells stably expressing Nrbf2-EGFP, Nrbf2-EGFP was primarily present in the cytosol fraction (**Figure 4a**), so was endogenous Nrbf2 in un-transfected HEK293 cells (**Figure 4b**).

Moreover, using confocal microscopy, we found that under nutrient-rich conditions, ectopically expressed Nrbf2-EGFP is primarily diffused in the cytosol, forming only a small numbers of cytoplasmic puncta; in contrast, upon 1 h starvation in Hank's buffer, the number of cytoplasmic Nrbf2-EGFP puncta significantly increased (**Figure 4c**). During autophagosome biogenesis, Atg14L localizes to the rough endoplasmic reticulum (ER) (25) and specifically the ER-mitochondria contact site (47), leading to the recruitment of Beclin 1 and Vps34 and subsequent production of PI3P in a Ulk1-FIP200 protein complex-dependent manner (25,26), forming the PI3P-enriched autophagosome initiation site (often referred to as isolation membrane, also termed omegasome due to its Ω -shape (48)). Ulk1 and Atg5, which synchronously form puncta in a PI3P-independent manner (49), accumulate in a PI3P-dependent manner to the PI3P-enriched autophagosome initiation sites (50). Subsequently, the Atg12-Atg5 and LC3-phosphatidylethanolamine (*i.e.*, LC3II) ubiquitin-like conjugation systems were recruited and assembled, leading to expansion of isolation membranes. Therefore, to further characterize the starvation-induced Nrbf2 punctate structures, we

examined the presence of isolation membrane markers on these structures. Of note, as starvation resulted in considerably more Nrbf2 puncta than nutrient-rich conditions, we monitored the colocalization of fluorescently-tagged Nrbf2 and isolation membrane markers in cells only under starvation conditions. We showed that ectopically expressed mCherry-Nrbf2, but not mCherry alone, colocalized with EGFP-Atg5 (**Figure 4d**); and ectopically expressed Nrbf2-EGFP, but not EGFP alone, colocalized with myc-Ulk1 (**Figure 4e**). We further showed that ectopically mCherry-Nrbf2, but not mCherry alone, colocalized with endogenous FIP200 (**Figure 4f**). Taken together, our results demonstrate colocalization of Nrbf2 with isolation membrane markers Atg5, Ulk1 and FIP200, suggesting involvement of Nrbf2 in autophagosome biogenesis.

Because the Ulk1-FIP200 protein complex is critical for initiating autophagosome biogenesis, we next investigated if the Ulk1 kinase activity or FIP200 was required for forming the Nrbf2 puncta. Ulk1 K46I was reported to be a dominant negative mutation, impairing Ulk1 kinase activity (51). Similarly, loss of FIP200 was reported to compromise Ulk1 stability, localization and activity (26,52,53). We showed that Nrbf2-EGFP puncta formed in both RPE-1 cells overexpressing Ulk1 K46I mutant (**Figure 4g**) and *FIP200*^{-/-} mouse embryonic fibroblasts (MEFs) (**Figure 4h**). These results suggest that in contrast to the Atg14L puncta, which cannot form in either HEK293 cells overexpressing dominant negative Ulk1 K46N mutant (25) or *FIP200*^{-/-} MEFs (26), the Nrbf2 puncta were able to form independent of the Ulk1 kinase activity or FIP200. Therefore, the involvement of Nrbf2 in autophagosome biogenesis does not depend on the Ulk1-FIP200 protein complex function.

E. Nrbf2 suppresses intracellular PI3P levels

The conversion of PtdIns to PI3P by Vps34 is important for autophagosome formation in both yeast and mammals (7,8,14). As our data presented above suggest that Nrbf2 is a component of the Atg14L-containing Beclin 1-Vps34 protein complex, we hypothesized that Nrbf2 may negatively regulate autophagic flux through suppressing the lipid kinase activity of Vps34. Utilizing an EGFP-2×FYVE plasmid which contains two consecutive specific PI3P-binding Fab1/YOTB/Vac1/EEA1 (FYVE) motifs (54,55), we showed that ectopically expressed mCherry-Nrbf2, but to a significantly lesser degree mCherry

alone, colocalized with EGFP-2×FYVE on punctate structures under serum-starvation conditions, suggesting localization of Nrbf2 on PI3P-enriched lipid domains (**Figure 5a**).

To investigate if Nrbf2 modulates intracellular PI3P levels, we initially used a semi-quantitative protein-lipid overlay assay to monitor intracellular PI3P levels in RPE-1 cells treated with non-targeting or Nrbf2 siRNA. The dot blot (layout shown in **Figure 5b**) clearly shows that the protein-lipid overlay assay specifically recognized PI3P, but not PI, PIP₃, PIP₂, or other PIPs (**Figure 5c, column 3**). Because we and others previously reported that Atg14L facilitates Vps34 lipid kinase activity (15,18,25), here we used Atg14L siRNA as a control. Our data demonstrate that Atg14L deficiency resulted in significantly decreased intracellular PI3P levels under serum-starvation conditions (**Figure 5d**), consistent with previous reports (15,18,25). We further showed that Nrbf2 deficiency, in contrary to Atg14L deficiency, led to increased intracellular PI3P levels ($p=0.002$ for nutrient-rich conditions and $p=0.1$ for serum-starvation conditions) (**Figure 5d**). Because the PI(3)P Mass Strip Kit for the protein-lipid overlay assay was discontinued by the company during our study, we later monitored intracellular PI3P levels using a replacement PI3P ELISA assay. Our ELISA data show that knocking down Nrbf2 by either the smartpool or 3'UTR Nrbf2 siRNA resulted in significantly increased intracellular PI3P levels under serum-starvation conditions, whereas under nutrient-rich conditions, the effect of Nrbf2 deficiency on intracellular PI3P levels was undetectable (**Figure 5e**). Because ELISA assays are generally thought to be more quantitative than dot blot assays (*e.g.*, the protein-lipid overlay assay), collectively, our results suggest that Nrbf2 suppresses intracellular PI3P levels under starvation conditions, likely through suppressing the Vps34-catalyzed conversion of PtdIns to PI3P, leading to negative regulation of autophagic flux.

F. Nrbf2 is required for the Atg14L-Vps34/Vps15 interactions

To further investigate the mechanism by which Nrbf2 regulates Vps34 activity, we performed IP to determine if Nrbf2 was required for protein-protein interactions within the Atg14L-containing Beclin 1-Vps34 protein complex. We first performed IP of endogenous Atg14L from RPE-1 cell treated with non-targeting, Nrbf2, Beclin 1, Vps34, or UVRAG siRNA. Our data

show that consistent with the literature (15,17), both Atg14L and UVRAG were unstable upon Beclin 1 or Vps34 siRNA treatment (**Figures 6a, INPUT, lanes 3-4**). We also observed that Atg14L was unable to pull down Nrbf2 upon Beclin 1 or Vps34 siRNA treatment (**Figure 6a, Atg14L IP, lanes 8-9**), which primarily reflected the loss of Atg14L as a result of Beclin 1 or Vps34 deficiency rather than the requirement of Beclin 1 or Vps34 for the Atg14L-Nrbf2 interaction. In addition, our data show that Atg14L was unable to pull down UVRAG (**Figure 6a, Atg14L IP, lane 6**), consistent with the notion that UVRAG and Atg14L are mutually exclusive (17,56). Most importantly, despite that Atg14L, Vps34 and Vps15 proteins were stable upon Nrbf2 siRNA treatment (**Figure 6a, INPUT, lanes 1-2**), endogenous Atg14L pulled down much less Vps34 or Vps15 upon Nrbf2 siRNA treatment as compared to upon non-targeting siRNA treatment (**Figure 6a, Atg14L IP, lanes 6-7**), suggesting that Nrbf2 is required for the Atg14L-Vps34/Vps15 interactions. Of note, our data also show that Nrbf2 was minimally needed for the Beclin 1-Atg14L interaction (**Figure 3d, Beclin 1 IP, lanes 5-6; Figure 6a, Atg14L IP, lanes 6-7**).

To further examine the requirement of Nrbf2 for the Atg14L-Vps34 interaction, we performed IP of endogenous Vps34 from RPE-1 cell treated with non-targeting, Nrbf2, or Beclin 1 siRNA. Our data show that the Vps34-UVRAG interaction was not changed upon Nrbf2 siRNA treatment (**Figure 6b, Vps34 IP, lanes 4-5**); in contrast, despite that both Atg14L and Vps34 proteins were stable upon Nrbf2 siRNA treatment (**Figure 6b, INPUT, lanes 1-2**), endogenous Vps34 pulled down much less Atg14L upon Nrbf2 siRNA treatment as compared to upon non-targeting siRNA treatment (**Figure 6b, Vps34 IP, lanes 4-5**). These results further support that Nrbf2 is required for the Atg14L-Vps34 interaction. In addition, Nrbf2 appears to be required for the Beclin 1-Vps34 interaction to a much lesser degree (**Figure 6b, Vps34 IP, lanes 4-5**). Furthermore, despite that Nrbf2, Vps34 and Vps15 protein levels were unchanged upon Beclin 1 deficiency (**Figure 6b, INPUT, Lanes 1 & 3**), the Nrbf2-Vps34 interaction or the Vps34-Vps15 interaction was abolished as a result of Beclin 1 siRNA treatment (**Figure 6b, Vps34 IP, lanes 4 & 6**), suggesting that Beclin 1 is required for Vps34 to interact with other components of the Beclin 1-Vps34 protein-protein interaction network.

Discussion

To elucidate the molecular details of autophagy regulation by the Beclin 1-Vps34 protein-protein interaction network, we set out to identify novel components in the network and characterized their roles in regulating autophagy (15). To this end, we identified Nrbf2 as a Beclin 1-interacting protein with its N-terminus required for binding to Beclin 1, and determined a novel role for Nrbf2 in negatively regulating autophagic flux. Using endogenous IP, we showed that Nrbf2 interacted with Beclin1, Vps34 and Vps15, the components of the core complex in the Beclin 1-Vps34 protein-protein interaction network. Interestingly, Nrbf2 also interacted with Atg14L, the adaptor to recruit the core complex for autophagosome biogenesis, but not UVRAG, the adaptor to recruit the core complex for endocytic trafficking. Moreover, Atg14L was required for the Beclin 1-Nrbf2 interaction, suggesting that Nrbf2 may interact with Beclin 1 through Atg14L. In addition, ectopically expressed Nrbf2 was colocalized with either ectopically expressed Atg14L alone or co-expressed Beclin 1 and Atg14L on cytoplasmic punctate structures. Taken together, we hypothesize that Nrbf2, by being a component of the Atg14L-containing Beclin 1-Vps34 protein complex, was involved in autophagosome biogenesis. Indeed, our data show that ectopically expressed Nrbf2 formed cytoplasmic puncta positive for isolation membrane markers Atg5, Ulk1 and FIP200 in a process that was independent of the Ulk1 kinase activity or FIP200. Therefore, our current working model for the role of Nrbf2 in autophagy is that Nrbf2 likely suppresses autophagy through negatively regulating Atg14L-containing Beclin 1-Vps34 protein complex-mediated autophagosome biogenesis, although our results do not exclude additional roles for Nrbf2 in autophagosome maturation.

To unravel the molecular mechanism by which Nrbf2 negatively regulated autophagosome biogenesis and autophagy, we showed that Nrbf2 localized on PI3P-enriched lipid domains and suppressed intracellular PI3P levels, consistent with a potential role of Nrbf2 in inhibiting Vps34 activity. We further showed that Nrbf2 was critical for the Atg14L-Vps34/Vps15 interactions, whereas the Beclin 1-Atg14L or Beclin1/Vps34-UVRAG interactions were unaffected by Nrbf2 deficiency. We summarize the protein-protein

interactions identified in this work in **Figure 6c**. It is possible that the Nrbf2-mediated Atg14L-Vps34/Vps15 interactions may contribute to the role of Nrbf2 in suppressing Vps34 activity through a conformational regulation-based mechanism. Therefore, in our current working model, we propose that Nrbf2 modulates protein-protein interactions in the Atg14L-containing Beclin 1-Vps34 protein complex, leading to the suppression of Vps34 activity, autophagosome biogenesis and autophagic flux.

The roles of the Beclin 1-Vps34 protein-protein interaction network are largely context-dependent, as components of the Beclin 1-Vps34 protein-protein interaction network have different, even opposing effects on autophagy. For example, Vps34 is essential for autophagy (7,8,14); paradoxically, during amino acid stimulation, Vps34 positively regulates mTOR complex 1, leading to autophagy inhibition (57-59). As another example, Beclin 1, when interacting with Atg14L, promotes autophagosome biogenesis (15-18); in contrast, Beclin 1 is involved in inhibition of autophagic activity when interacting with either 14-3-3 (60) (as a result of Beclin 1 phosphorylation by Akt) or Bcl-2 (24) (interaction weakened by death-associated protein kinase-mediated Beclin 1 phosphorylation (61,62)). In addition, UVRAG has been suggested to either direct Beclin 1 and Vps34 to endocytic trafficking (17) or promote autophagosome maturation (27) and, with some controversy, autophagosome biogenesis (17,28). Therefore, the Beclin 1-Vps34 protein-protein interaction network appears to be dynamic, serving as a key regulatory hub to integrate extracellular and intracellular cues for tight control of autophagic activity. Based on our data presented here, Nrbf2 is an important component of this context-dependent Beclin 1-Vps34 protein-protein interaction network; under certain conditions, such as reported in this work, Nrbf2 negatively regulates autophagy and likely Vps34 activity through modulating protein-protein interactions in the Beclin 1-Vps34 network.

As a final note, while our manuscript was under review, three studies reported the identification of mouse (63) and human (64) Nrbf2 and the yeast ortholog Atg38 (65) as a component of the Beclin 1/Vps30-Vps34 protein-protein interaction network. Our biochemical data are largely consistent with the above reports that Nrbf2 is primarily a component of the Atg14L/Atg14-containing Beclin 1/Vps30-Vps34

complex and critical for the assembly of the Atg14L/Atg14-Beclin1/Vps30 and Vps34-Vps15 sub-complexes. Our results are also consistent with the above reports that Nrbf2 is involved in autophagosome biogenesis. However, in contrary to the above reports showing a positive role of Nrbf2 in regulating autophagy, using a variety of independent autophagic flux assays, we showed that human Nrbf2 suppressed autophagic flux in RPE-1 and HepG2 cells. Although we do not understand what cause(s) the difference in our and the other groups' studies, we postulate that the discrepancy is likely rooted in the context-dependency of autophagy regulation. For example, the MIT and CCD domains of yeast Atg38 are evolutionarily more divergent from those of the mammalian Nrbf2 (**Figure 1d**). In particular, the CCD of yeast Atg38 lacks the five leucines that are consecutive at every seven residues in the mammalian Nrbf2 CCD (**Figure 1d**). These sequence deviations of yeast Atg38 from mammalian Nrbf2 may result in alteration in function. Moreover, we also participated in one of the reported study where Nrbf2 was observed to enhance autophagy and Vps34 activity in NIH 3T3 cells and MEFs (64). Even in our own hands, Nrbf2 siRNA treated NIH 3T3 cells showed increased p62 levels (data not shown). Therefore, it is possible that Nrbf2 may function differently in human versus mouse cells. Supporting this notion, it has been reported that expression levels of Beclin 1 and Atg14L, as well as the stoichiometry of the Beclin 1-Vps34 protein complexes, were drastically different in mouse (NIH 3T3 and MEFs) and human (Hela) cell lines (40). Furthermore, our study utilized siRNA to transiently (~3 days) knocking down Nrbf2, while all the above-mentioned reports utilized either genetic knockout (64,65) or stable knockdown (63). It is possible that lacking Nrbf2 for an extended period of time may alter the cellular context. In short, Nrbf2 is an important player for tight autophagy regulation, maybe in a species-, cell type-, or stress-specific manner. Further

investigation is necessary to reveal the context-dependency of autophagy regulation by Nrbf2.

Acknowledgements

This work was supported by National Institutes of Health Grants P20GM103486 (Q.J.W.), RR00862 and RR022220 (B.T.C.), and by the Ellison Medical Foundation (Q.J.W.). We thank J. Guan (University of Cincinnati) for *FIP200*^{+/+} and *FIP200*^{-/-} MEF cells, H. Stenmark (University of Oslo) for the EGFP-2xFYVE plasmid, S. Tooze (London Research Institute) for the myc-Ulk1 and myc-Ulk1 K46I constructs, Z. Yue (Mount Sinai School of Medicine) for the mouse Nrbf2-EGFP, Atg14L-AsRed and FLAG-Beclin 1 plasmids, and X. Jiang (Memorial Sloan Kettering Cancer Center) for the EGFP-Atg5 plasmid. We thank the Imaging Core of the NIH Center of Biomedical Research Excellence (COBRE) at the University of Kentucky for providing the access to microscopes. We also thank J. Simpson for technical support and Drs. K.L. Guan and J. Kim for helpful tips for Beclin 1-Vps34 complex immunoprecipitation.

Author contributions

Q.J.W. conceived the project and coordinated all efforts in the study. Y.Z., D.H.M., L.J., B.T.C. and Q.J.W. designed the project. Y.Z., D.H.M., L.J., M.S.P., S.K.K., Y.J.F., E.A.M and Q.J.W. carried out the experiments. Y.Z., H.L.W. and Q.J.W. analyzed the data. Y.Z., D.H.M, L.J. and Q.J.W. wrote the paper. For experiments, D.H.M., L.J. and M.S.P. generated the Nrbf2 plasmids. Y.Z. contributed to Figures 2, 3, 5 and 6; D.H.M. contributed to Figures 3 and 4; M.S.P. contributed to Figures 1 and 3; Y.J.F. and L.J. contributed to Figure 1; S.K.K. and E.A.M. contributed to Figure 2; and Q.J.W. contributed to Figures 1, 2, 3, and 5.

Conflict of Interest

The authors declare no conflict of interest.

References

1. Suzuki, K., and Ohsumi, Y. (2007) Molecular machinery of autophagosome formation in yeast, *Saccharomyces cerevisiae*. *FEBS Lett* **581**, 2156-2161
2. Mizushima, N., Levine, B., Cuervo, A. M., and Klionsky, D. J. (2008) Autophagy fights disease through cellular self-digestion. *Nature* **451**, 1069-1075
3. Liu, Y., Shoji-Kawata, S., Sumpter, R. M., Jr., Wei, Y., Ginet, V., Zhang, L., Posner, B., Tran, K. A., Green, D. R., Xavier, R. J., Shaw, S. Y., Clarke, P. G., Puyal, J., and Levine, B. (2013) Autosis is a Na⁺,K⁺-ATPase-regulated form of cell death triggered by autophagy-inducing peptides, starvation, and hypoxia-ischemia. *Proc Natl Acad Sci U S A* **110**, 20364-20371
4. Liang, X. H., Jackson, S., Seaman, M., Brown, K., Kempkes, B., Hibshoosh, H., and Levine, B. (1999) Induction of autophagy and inhibition of tumorigenesis by beclin 1. *Nature* **402**, 672-676
5. Liang, X. H., Kleeman, L. K., Jiang, H. H., Gordon, G., Goldman, J. E., Berry, G., Herman, B., and Levine, B. (1998) Protection against fatal Sindbis virus encephalitis by beclin, a novel Bcl-2-interacting protein. *J Virol* **72**, 8586-8596
6. Maiuri, M. C., Le Toumelin, G., Criollo, A., Rain, J. C., Gautier, F., Juin, P., Tasdemir, E., Pierron, G., Troulinaki, K., Tavernarakis, N., Hickman, J. A., Geneste, O., and Kroemer, G. (2007) Functional and physical interaction between Bcl-X(L) and a BH3-like domain in Beclin-1. *EMBO J* **26**, 2527-2539
7. Stack, J. H., and Emr, S. D. (1994) Vps34p required for yeast vacuolar protein sorting is a multiple specificity kinase that exhibits both protein kinase and phosphatidylinositol-specific PI 3-kinase activities. *J Biol Chem* **269**, 31552-31562
8. Volinia, S., Dhand, R., Vanhaesebroeck, B., MacDougall, L. K., Stein, R., Zvelebil, M. J., Domin, J., Panaretou, C., and Waterfield, M. D. (1995) A human phosphatidylinositol 3-kinase complex related to the yeast Vps34p-Vps15p protein sorting system. *EMBO J* **14**, 3339-3348
9. Obara, K., Sekito, T., and Ohsumi, Y. (2006) Assortment of phosphatidylinositol 3-kinase complexes--Atg14p directs association of complex I to the pre-autophagosomal structure in *Saccharomyces cerevisiae*. *Mol Biol Cell* **17**, 1527-1539
10. Kihara, A., Noda, T., Ishihara, N., and Ohsumi, Y. (2001) Two distinct Vps34 phosphatidylinositol 3-kinase complexes function in autophagy and carboxypeptidase Y sorting in *Saccharomyces cerevisiae*. *J Cell Biol* **152**, 519-530
11. Funderburk, S. F., Wang, Q. J., and Yue, Z. (2010) The Beclin 1-VPS34 complex - at the crossroads of autophagy and beyond. *Trends Cell Biol* **20**, 355-362
12. He, C., and Levine, B. (2010) The Beclin 1 interactome. *Curr Opin Cell Biol* **22**, 140-149
13. Kang, R., Zeh, H. J., Lotze, M. T., and Tang, D. (2011) The Beclin 1 network regulates autophagy and apoptosis. *Cell Death Differ* **18**, 571-580
14. Jaber, N., Dou, Z., Chen, J. S., Catanzaro, J., Jiang, Y. P., Ballou, L. M., Selinger, E., Ouyang, X., Lin, R. Z., Zhang, J., and Zong, W. X. (2012) Class III PI3K Vps34 plays an essential role in autophagy and in heart and liver function. *Proc Natl Acad Sci U S A* **109**, 2003-2008
15. Zhong, Y., Wang, Q. J., Li, X., Yan, Y., Backer, J. M., Chait, B. T., Heintz, N., and Yue, Z. (2009) Distinct regulation of autophagic activity by Atg14L and Rubicon associated with Beclin 1-phosphatidylinositol-3-kinase complex. *Nat Cell Biol* **11**, 468-476
16. Matsunaga, K., Saitoh, T., Tabata, K., Omori, H., Satoh, T., Kurotori, N., Maejima, I., Shirahama-Noda, K., Ichimura, T., Isobe, T., Akira, S., Noda, T., and Yoshimori, T. (2009) Two Beclin 1-binding proteins, Atg14L and Rubicon, reciprocally regulate autophagy at different stages. *Nat Cell Biol* **11**, 385-396
17. Itakura, E., Kishi, C., Inoue, K., and Mizushima, N. (2008) Beclin 1 forms two distinct phosphatidylinositol 3-kinase complexes with mammalian Atg14 and UVRAG. *Mol Biol Cell* **19**, 5360-5372
18. Sun, Q., Fan, W., Chen, K., Ding, X., Chen, S., and Zhong, Q. (2008) Identification of Barkor as a mammalian autophagy-specific factor for Beclin 1 and class III phosphatidylinositol 3-kinase. *Proc Natl Acad Sci U S A* **105**, 19211-19216

19. Dou, Z., Chattopadhyay, M., Pan, J. A., Guerriero, J. L., Jiang, Y. P., Ballou, L. M., Yue, Z., Lin, R. Z., and Zong, W. X. (2010) The class IA phosphatidylinositol 3-kinase p110-beta subunit is a positive regulator of autophagy. *J Cell Biol* **191**, 827-843
20. Fimia, G. M., Stoykova, A., Romagnoli, A., Giunta, L., Di Bartolomeo, S., Nardacci, R., Corazzari, M., Fuoco, C., Ucar, A., Schwartz, P., Gruss, P., Piacentini, M., Chowdhury, K., and Cecconi, F. (2007) Ambra1 regulates autophagy and development of the nervous system. *Nature* **447**, 1121-1125
21. Ropolo, A., Grasso, D., Pardo, R., Sacchetti, M. L., Archange, C., Lo Re, A., Seux, M., Nowak, J., Gonzalez, C. D., Iovanna, J. L., and Vaccaro, M. I. (2007) The pancreatitis-induced vacuole membrane protein 1 triggers autophagy in mammalian cells. *J Biol Chem* **282**, 37124-37133
22. Molejon, M. I., Ropolo, A., Re, A. L., Boggio, V., and Vaccaro, M. I. (2013) The VMP1-Beclin 1 interaction regulates autophagy induction. *Scientific reports* **3**, 1055
23. Tang, D., Kang, R., Livesey, K. M., Cheh, C. W., Farkas, A., Loughran, P., Hoppe, G., Bianchi, M. E., Tracey, K. J., Zeh, H. J., 3rd, and Lotze, M. T. (2010) Endogenous HMGB1 regulates autophagy. *J Cell Biol* **190**, 881-892
24. Pattingre, S., Tassa, A., Qu, X., Garuti, R., Liang, X. H., Mizushima, N., Packer, M., Schneider, M. D., and Levine, B. (2005) Bcl-2 antiapoptotic proteins inhibit Beclin 1-dependent autophagy. *Cell* **122**, 927-939
25. Matsunaga, K., Morita, E., Saitoh, T., Akira, S., Ktistakis, N. T., Izumi, T., Noda, T., and Yoshimori, T. (2010) Autophagy requires endoplasmic reticulum targeting of the PI3-kinase complex via Atg14L. *J Cell Biol* **190**, 511-521
26. Itakura, E., and Mizushima, N. (2010) Characterization of autophagosome formation site by a hierarchical analysis of mammalian Atg proteins. *Autophagy* **6**, 764-776
27. Liang, C., Lee, J. S., Inn, K. S., Gack, M. U., Li, Q., Roberts, E. A., Vergne, I., Deretic, V., Feng, P., Akazawa, C., and Jung, J. U. (2008) Beclin1-binding UVRAG targets the class C Vps complex to coordinate autophagosome maturation and endocytic trafficking. *Nat Cell Biol* **10**, 776-787
28. Liang, C., Feng, P., Ku, B., Dotan, I., Canaani, D., Oh, B. H., and Jung, J. U. (2006) Autophagic and tumour suppressor activity of a novel Beclin1-binding protein UVRAG. *Nat Cell Biol* **8**, 688-699
29. Aita, V. M., Liang, X. H., Murty, V. V., Pincus, D. L., Yu, W., Cayanis, E., Kalachikov, S., Gilliam, T. C., and Levine, B. (1999) Cloning and genomic organization of beclin 1, a candidate tumor suppressor gene on chromosome 17q21. *Genomics* **59**, 59-65
30. Yue, Z., Jin, S., Yang, C., Levine, A. J., and Heintz, N. (2003) Beclin 1, an autophagy gene essential for early embryonic development, is a haploinsufficient tumor suppressor. *Proc Natl Acad Sci U S A* **100**, 15077-15082
31. Qu, X., Yu, J., Bhagat, G., Furuya, N., Hibshoosh, H., Troxel, A., Rosen, J., Eskelinen, E. L., Mizushima, N., Ohsumi, Y., Cattoretti, G., and Levine, B. (2003) Promotion of tumorigenesis by heterozygous disruption of the beclin 1 autophagy gene. *J Clin Invest* **112**, 1809-1820
32. Takahashi, Y., Coppola, D., Matsushita, N., Cialing, H. D., Sun, M., Sato, Y., Liang, C., Jung, J. U., Cheng, J. Q., Mule, J. J., Pledger, W. J., and Wang, H. G. (2007) Bif-1 interacts with Beclin 1 through UVRAG and regulates autophagy and tumorigenesis. *Nat Cell Biol* **9**, 1142-1151
33. Qu, X., Zou, Z., Sun, Q., Luby-Phelps, K., Cheng, P., Hogan, R. N., Gilpin, C., and Levine, B. (2007) Autophagy gene-dependent clearance of apoptotic cells during embryonic development. *Cell* **128**, 931-946
34. Melendez, A., Tallozy, Z., Seaman, M., Eskelinen, E. L., Hall, D. H., and Levine, B. (2003) Autophagy genes are essential for dauer development and life-span extension in *C. elegans*. *Science* **301**, 1387-1391
35. Shibata, M., Lu, T., Furuya, T., Degtarev, A., Mizushima, N., Yoshimori, T., MacDonald, M., Yankner, B., and Yuan, J. (2006) Regulation of intracellular accumulation of mutant Huntingtin by Beclin 1. *J Biol Chem* **281**, 14474-14485
36. Yue, Z., Horton, A., Bravin, M., DeJager, P. L., Selimi, F., and Heintz, N. (2002) A novel protein complex linking the delta 2 glutamate receptor and autophagy: implications for neurodegeneration in lurcher mice. *Neuron* **35**, 921-933

37. Diskin, T., Tal-Or, P., Erlich, S., Mizrachi, L., Alexandrovich, A., Shohami, E., and Pinkas-Kramarski, R. (2005) Closed head injury induces upregulation of Beclin 1 at the cortical site of injury. *J Neurotrauma* **22**, 750-762
38. Yasuno, H., Masuda, N., Furusawa, T., Tsukamoto, T., Sadano, H., and Osumi, T. (2000) Nuclear receptor binding factor-2 (NRBF-2), a possible gene activator protein interacting with nuclear hormone receptors. *Biochim Biophys Acta* **1490**, 189-197
39. Flores, A. M., Li, L., and Aneskievich, B. J. (2004) Isolation and functional analysis of a keratinocyte-derived, ligand-regulated nuclear receptor comodulator. *J Invest Dermatol* **123**, 1092-1101
40. Kim, J., Kim, Y. C., Fang, C., Russell, R. C., Kim, J. H., Fan, W., Liu, R., Zhong, Q., and Guan, K. L. (2013) Differential regulation of distinct Vps34 complexes by AMPK in nutrient stress and autophagy. *Cell* **152**, 290-303
41. Gao, W., Shen, Z., Shang, L., and Wang, X. (2011) Upregulation of human autophagy-initiation kinase ULK1 by tumor suppressor p53 contributes to DNA-damage-induced cell death. *Cell Death Differ* **18**, 1598-1607
42. Behrends, C., Sowa, M. E., Gygi, S. P., and Harper, J. W. (2010) Network organization of the human autophagy system. *Nature* **466**, 68-76
43. Bjorkoy, G., Lamark, T., Brech, A., Outzen, H., Perander, M., Overvatn, A., Stenmark, H., and Johansen, T. (2005) p62/SQSTM1 forms protein aggregates degraded by autophagy and has a protective effect on huntingtin-induced cell death. *J Cell Biol* **171**, 603-614
44. Klionsky, D. J., Elazar, Z., Seglen, P. O., and Rubinsztein, D. C. (2008) Does bafilomycin A(1) block the fusion of autophagosomes with lysosomes? *Autophagy* **4**, 849-850
45. Menzies, F. M., Moreau, K., Puri, C., Renna, M., and Rubinsztein, D. C. (2012) Measurement of autophagic activity in mammalian cells. *Curr Protoc Cell Biol* **Chapter 15**, Unit 15-16
46. Mizushima, N., Yoshimori, T., and Levine, B. (2010) Methods in mammalian autophagy research. *Cell* **140**, 313-326
47. Hamasaki, M., Furuta, N., Matsuda, A., Nezu, A., Yamamoto, A., Fujita, N., Oomori, H., Noda, T., Haraguchi, T., Hiraoka, Y., Amano, A., and Yoshimori, T. (2013) Autophagosomes form at ER-mitochondria contact sites. *Nature* **495**, 389-393
48. Axe, E. L., Walker, S. A., Manifava, M., Chandra, P., Roderick, H. L., Habermann, A., Griffiths, G., and Ktistakis, N. T. (2008) Autophagosome formation from membrane compartments enriched in phosphatidylinositol 3-phosphate and dynamically connected to the endoplasmic reticulum. *J Cell Biol* **182**, 685-701
49. Koyama-Honda, I., Itakura, E., Fujiwara, T. K., and Mizushima, N. (2013) Temporal analysis of recruitment of mammalian ATG proteins to the autophagosome formation site. *Autophagy* **9**, 1491-1499
50. Karaniasios, E., Stapleton, E., Manifava, M., Kaizuka, T., Mizushima, N., Walker, S. A., and Ktistakis, N. T. (2013) Dynamic association of the ULK1 complex with omegasomes during autophagy induction. *J Cell Sci* **126**, 5224-5238
51. Chan, E. Y., Longatti, A., McKnight, N. C., and Tooze, S. A. (2009) Kinase-inactivated ULK proteins inhibit autophagy via their conserved C-terminal domains using an Atg13-independent mechanism. *Mol Cell Biol* **29**, 157-171
52. Ganley, I. G., Lam du, H., Wang, J., Ding, X., Chen, S., and Jiang, X. (2009) ULK1.ATG13.FIP200 complex mediates mTOR signaling and is essential for autophagy. *J Biol Chem* **284**, 12297-12305
53. Hara, T., Takamura, A., Kishi, C., Iemura, S., Natsume, T., Guan, J. L., and Mizushima, N. (2008) FIP200, a ULK-interacting protein, is required for autophagosome formation in mammalian cells. *J Cell Biol* **181**, 497-510
54. Stenmark, H., Aasland, R., Toh, B. H., and DArrigo, A. (1996) Endosomal localization of the autoantigen EEA1 is mediated by a zinc-binding FYVE finger. *Journal of Biological Chemistry* **271**, 24048-24054
55. Gilooly, D. J., Morrow, I. C., Lindsay, M., Gould, R., Bryant, N. J., Gaullier, J. M., Parton, R. G., and Stenmark, H. (2000) Localization of phosphatidylinositol 3-phosphate in yeast and mammalian cells. *EMBO J* **19**, 4577-4588

56. Li, X., He, L., Che, K. H., Funderburk, S. F., Pan, L., Pan, N., Zhang, M., Yue, Z., and Zhao, Y. (2012) Imperfect interface of Beclin1 coiled-coil domain regulates homodimer and heterodimer formation with Atg14L and UVRAG. *Nat Commun* **3**, 662
57. Backer, J. M. (2008) The regulation and function of Class III PI3Ks: novel roles for Vps34. *Biochem J* **410**, 1-17
58. Byfield, M. P., Murray, J. T., and Backer, J. M. (2005) hVps34 is a nutrient-regulated lipid kinase required for activation of p70 S6 kinase. *J Biol Chem* **280**, 33076-33082
59. Nobukuni, T., Joaquin, M., Roccio, M., Dann, S. G., Kim, S. Y., Gulati, P., Byfield, M. P., Backer, J. M., Natt, F., Bos, J. L., Zwartkuis, F. J., and Thomas, G. (2005) Amino acids mediate mTOR/raptor signaling through activation of class 3 phosphatidylinositol 3OH-kinase. *Proc Natl Acad Sci U S A* **102**, 14238-14243
60. Wang, R. C., Wei, Y., An, Z., Zou, Z., Xiao, G., Bhagat, G., White, M., Reichelt, J., and Levine, B. (2012) Akt-mediated regulation of autophagy and tumorigenesis through Beclin 1 phosphorylation. *Science* **338**, 956-959
61. Zalckvar, E., Berissi, H., Eisenstein, M., and Kimchi, A. (2009) Phosphorylation of Beclin 1 by DAP-kinase promotes autophagy by weakening its interactions with Bcl-2 and Bcl-XL. *Autophagy* **5**, 720-722
62. Zalckvar, E., Berissi, H., Mizrachy, L., Idelchuk, Y., Koren, I., Eisenstein, M., Sabanay, H., Pinkas-Kramarski, R., and Kimchi, A. (2009) DAP-kinase-mediated phosphorylation on the BH3 domain of beclin 1 promotes dissociation of beclin 1 from Bcl-XL and induction of autophagy. *EMBO Rep* **10**, 285-292
63. Cao, Y., Wang, Y., Abi Saab, W. F., Yang, F., Pessin, J. E., and Backer, J. M. (2014) NRBF2 regulates macroautophagy as a component of Vps34 Complex I. *Biochem J* **461**, 315-322
64. Lu, J., He, L., Behrends, C., Araki, M., Araki, K., Wang, Q. J., Catanzaro, J. M., Friedman, S. L., Zong, W. X., Fiel, M. I., Li, M., and Yue, Z. (2014) NRBF2 regulates autophagy and prevents liver injury by modulating Atg14L-linked phosphatidylinositol-3 kinase III activity. *Nat Commun* **5**, 3920-3934
65. Araki, Y., Ku, W. C., Akioka, M., May, A. I., Hayashi, Y., Arisaka, F., Ishihama, Y., and Ohsumi, Y. (2013) Atg38 is required for autophagy-specific phosphatidylinositol 3-kinase complex integrity. *J Cell Biol* **203**, 299-313

Figure Legends

Figure 1. Identification of Nrbf2 as a novel Beclin 1-interacting protein. **(a)** Anti-EGFP antibody pulled down endogenous Beclin 1 and Vps34 in HEK293 cells stably expressing mouse Nrbf2-EGFP under both nutrient-rich and serum-starvation conditions. Immunoprecipitated Nrbf2-EGFP and EGFP were labeled in the anti-GFP blot. **(b)** Anti-Nrbf2 antibody pulled down endogenous Beclin 1, Vps34 and Vps15 from RPE-1 cells transfected with non-targeting siRNA but not from those transfected with the smartpool Nrbf2 siRNA. Of note, both cell extracts before IP (labeled INPUT) contain similar levels of Beclin 1, Vps34, Vps15 and actin. **(c)** Human Nrbf2 domain structures and diagrams of the C-terminal Cycle3 GFP-tagged full length human Nrbf2 and truncation mutants (M1-M6) of Nrbf2. **(d)** Sequence alignment of Nrbf2 MIT and CCD domains from different species. The five key leucines in the CCD domain are marked by red asterisks. Note that Atg38, the yeast ortholog of Nrbf2, has low sequence homology to the mammalian Nrbf2, particularly lacking the above mentioned five key leucines in the CCD domain. **(e)** Anti-GFP IP of GFP-tagged full length and mutant Nrbf2 constructs from HepG2 cells revealed that the N-terminal 120 residues of Nrbf2 were required and sufficient for the Nrbf2-Beclin 1 interaction. Red asterisks mark the IgG bands. GFP-tagged full length and mutant Nrbf2 constructs in the INPUT were probed with anti-GFP antibody.

Figure 2. Characterization of Nrbf2 as a negative regulator for autophagic flux under both nutrient-rich and starvation conditions in human cell lines. Western blot analysis of p62 in **(a)** RPE-1 and **(c)** HepG2 cells transfected with non-targeting control (Ctl) siRNA, human smartpool (sp) and 3'UTR Nrbf2 showed decreased p62 levels upon Nrbf2 siRNA treatment. For **(a)**, cells were grown under nutrient-rich or 1 h Hank's buffer starvation conditions. For **(c)**, cells were grown under nutrient-rich conditions. **(b)** qRT-PCR quantification of the relative p62 transcript levels in the RPE-1 cells transfected with Ctl, Nrbf2 sp, and Nrbf2 3'UTR siRNAs. **(d)** Western blot analysis of p62 levels in RPE-1 cells transfected with Ctl or smartpool Nrbf2 siRNA showed decreased p62 levels upon Nrbf2 siRNA treatment under both nutrient-rich and 18 h serum-starvation conditions. **(e)** Western blot analysis of LC3II levels in RPE-1 cells transfected with Ctl siRNA or smartpool Nrbf2 siRNA, and treated either without or with 200 nM Baf showed greater Baf-induced increase of LC3II levels upon Nrbf2 siRNA treatment under both nutrient-rich and 18 h serum-starvation conditions. **(f)** Western blot analysis of LC3II levels in RPE-1 cells transfected with mCherry empty vector or mCherry-tagged human Nrbf2, and treated either without or with 200 nM Baf showed lesser Baf-induced increase of LC3II levels upon Nrbf2 overexpression under both nutrient-rich or 18 h serum-starvation conditions. Note that statistical significance for the LC3II assays in **(e-f)** is lower than that for the p62 assay in **(d)**, likely due to fewer numbers of independent experiments. **(g)** Long-lived protein degradation rate, measured by ^{14}C -Leu radioactivity in the medium normalized to total ^{14}C -Leu radioactivity in both the medium and the cells, increased upon Nrbf2 siRNA treatment under both nutrient-rich and serum-starvation conditions. For all quantifications in **Figure 2**, means and standard errors were plotted with means labeled.

Figure 3. Nrbf2 is a component of the Atg14L-containing Beclin 1-Vps34 protein complex. **(a)** Transiently expressed EGFP-tagged full length Atg14L, but not the CCD domain deletion mutants of Atg14L, pulled down endogenous Nrbf2 in HeLa cells. Immunoprecipitated EGFP-tagged full length and mutant Atg14L were probed with anti-GFP antibody. **(b)** Ectopically expressed mCherry-Nrbf2 colocalized with Atg14L-EGFP on punctate structures (pointed to by arrows) in RPE-1 cells under nutrient-rich and 18 h serum starvation conditions. In contrast, mCherry alone showed diffused cytoplasmic and nuclear localization. Scale bars, 10 μm . **(c)** Quantification of colocalization of mCherry or mCherry-Nrbf2 with Atg14L-EGFP, as measured by the percentage of Atg14L-EGFP puncta that are either mCherry- or mCherry-Nrbf2-positive. Cells with more than 5 Atg14L-EGFP puncta were used for quantification. The numbers of cells used for quantification were 5 (for mCherry, nutrient-rich), 7 (for mCherry, serum starvation), 9 (for mCherry-Nrbf2, nutrient-rich), and 7 (for mCherry-Nrbf2, serum starvation). These cell numbers are sufficient to reveal statistical significance of colocalization between mCherry-Nrbf2 and Atg14L-EGFP, using a two-tailed Student's t-test. **(d)** Anti-Beclin 1 IP from RPE-1 cell treated with non-targeting, Nrbf2, Atg14L, or UVRAG siRNA. **(e)** Anti-Nrbf2 IP from RPE-1 cell

treated with non-targeting, Nrbf2, Atg14L, or Vps34 siRNA. Note that Vps34 siRNA treatment led to unstable Nrbf2, Beclin 1, Atg14L, UVRAG and Vps15, whereas Atg14L siRNA treatment only slightly destabilize Beclin 1 and did not destabilize Nrbf2, UVRAG, Vps34 or Vps15. For (d-e), interactions that required Atg14L were marked by blue asterisks. (f) Ectopically expressed Nrbf2-EGFP, Atg14L-AsRed and FLAG-Beclin 1 colocalized on punctate structures in RPE-1 cells under 1 h Hank's buffer starvation conditions. Scale bars, 20 μ m.

Figure 4. Nrbf2 forms cytoplasmic puncta that are positive for isolation membrane markers in RPE-1 cells. Subcellular fractionation revealed that both (a) stably expressed Nrbf2-EGFP and (b) endogenous Nrbf2 were primarily localized in the cytosol in HEK293 cells under nutrient-rich conditions. A1 — cytosolic fraction as marked by SOD1; A2 — membrane fraction as marked by EGFR; A3 — soluble nuclear fraction as marked by SP1; A4 — chromatin-bound nuclear fraction as marked by histone H3; A5 — cytoskeletal fraction; and A6 — pellet fraction. (c) Ectopically expressed Nrbf2-EGFP formed cytoplasmic punctate structures under both nutrient-rich and Hank's buffer starvation conditions. The numbers of cells used for quantification were 18 (for EGFP, nutrient-rich), 24 (for EGFP, Hank's buffer starvation), 22 (for Nrbf2-EGFP, nutrient-rich), and 22 (for Nrbf2-Nrbf2, Hanks's buffer starvation). (d) Ectopically expressed mCherry-Nrbf2 and EGFP-Atg5 colocalized on punctate structures under Hank's buffer starvation conditions. The numbers of cells used for quantification were 14 (for mCherry) and 12 (for mCherry-Nrbf2). (e) Ectopically expressed Nrbf2-EGFP and myc-tagged Ulk1 wild-type (WT) colocalized on punctate structures under Hank's buffer starvation conditions. The numbers of cells used for quantification were 9 (for EGFP) and 4 (for Nrbf2-EGFP). (f) Ectopically expressed mCherry-Nrbf2 and endogenous FIP200 colocalized on punctate structures under Hank's buffer starvation conditions. The numbers of cells used for quantification were 3 (for mCherry) and 8 (for mCherry-Nrbf2). (g) Ectopically expressed Nrbf2-EGFP and myc-tagged Ulk1 K46I mutant colocalized on punctate structures under Hank's buffer starvation conditions. The numbers of cells used for quantification were 6 (for EGFP) and 9 (for Nrbf2-EGFP). For (d-g), note that mCherry or EGFP was primarily diffused whereas mCherry-Nrbf2 or Nrbf2-EGFP formed puncta under Hank's buffer starvation conditions. (h) Ectopically expressed Nrbf2-EGFP formed cytoplasmic puncta in both *FIP200*^{+/+} and *FIP200*^{-/-} MEFs. The numbers of cells used for quantification were 6 (for EGFP, *FIP200*^{+/+}), 11 (for Nrbf2-EGFP, *FIP200*^{+/+}), 8 (for EGFP, *FIP200*^{-/-}), and 10 (for Nrbf2-EGFP, *FIP200*^{-/-}). Scale bars: 10 μ m for (c-f) and 20 μ m for (g-h).

Figure 5. Nrbf2 reduces intracellular PI3P levels in RPE-1 cells. (a) Ectopically expressed mCherry-Nrbf2 and EGFP-2xFYVE colocalized on punctate structures under serum starvation conditions. Scale bars: 10 μ m. The number of cells used for quantification was 18 for either mCherry or mCherry-Nrbf2. Note that because EGFP-2xFYVE was capable of sequestering cytoplasmic constituents, even mCherry alone formed some punctate structures that were positive for EGFP-2xFYVE. However, mCherry-Nrbf2 clearly formed more distinctive puncta and colocalized with EGFP-2xFYVE to a higher degree. (b-d) Monitoring intracellular PI3P levels in RPE-1 cells treated with non-targeting (Ctl), smartpool Nrbf2 and Atg14L siRNA respectively by protein-lipid overlay assay. (b) Layout of the PI(3)P Mass Strip. (c) A representative dot blot showing extracted acidic lipids as detected by enhanced chemiluminescence (ECL). Corresponding amounts of total proteins were labeled in parentheses. Note that PI, PIP₃, PIP₂ and other PIP controls in lane 3 and 0.5-1 pmol of PI3P in lane 2 showed barely detectable signals. (d) Comparison of extracted intracellular PI3P levels (normalized to total protein levels) upon non-targeting, Nrbf2 and Atg14L siRNA treatments for data collected in (c). Four independent experiments were performed. Means and standard errors were plotted with means labeled. (e) Comparison of extracted intracellular PI3P levels (normalized to total protein levels) upon non-targeting, smartpool and 3'UTR Nrbf2 siRNA respectively in RPE-1 cells using the PI(3)P Mass ELISA Kit. Six independent experiments were performed, with each experiment individually plotted to best show the effect of Nrbf2 siRNA treatment.

Figure 6. Nrbf2 is required for the Atg14L-Vps34/Vps15 interactions. (a) IP of endogenous Atg14L in RPE-1 cell treated with non-targeting, Nrbf2, Beclin 1, Vps34, or UVRAG siRNA under nutrient-rich

conditions. **(b)** IP of endogenous Vps34 in RPE-1 cell treated with non-targeting, Nrbf2, or Beclin 1 siRNA under nutrient-rich conditions. For **(a-b)**, interactions that required Nrbf2 and Beclin 1 were marked by red and green asterisks, respectively. **(c)** A diagram summarized the interactions identified in this work through endogenous IPs shown in **Figures 3d, 3e, 6a** and **6b**. Each arrow was pointed from bait to prey.

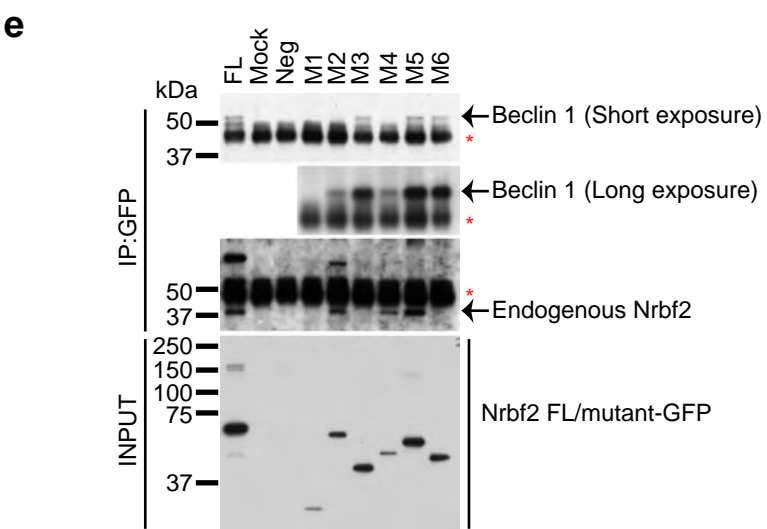
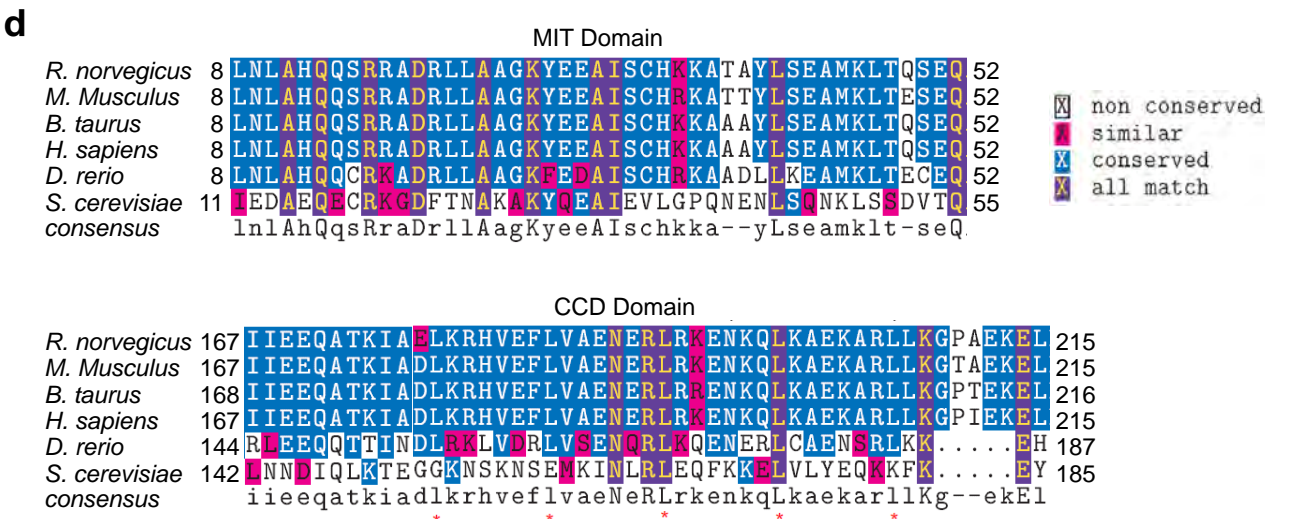
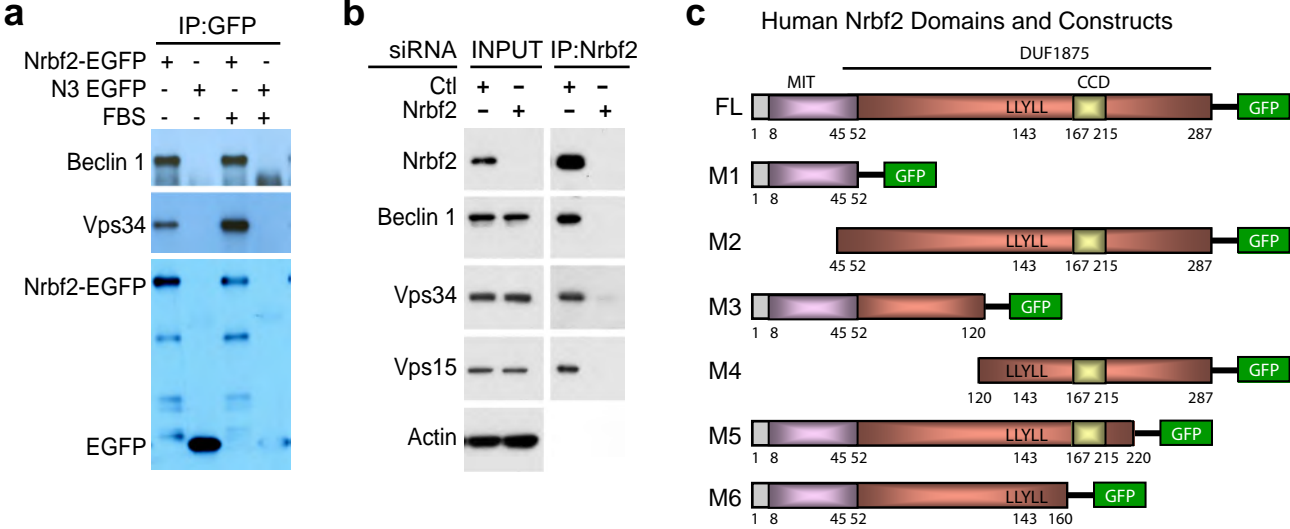


Figure 1

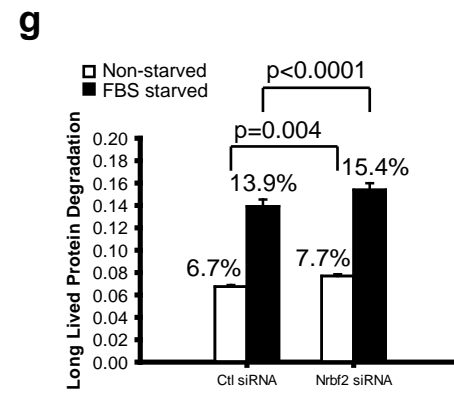
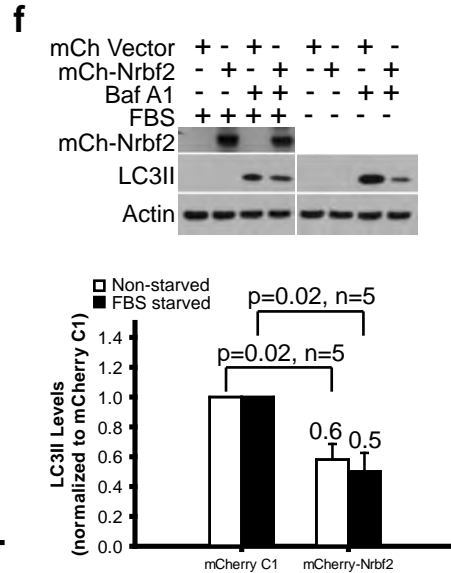
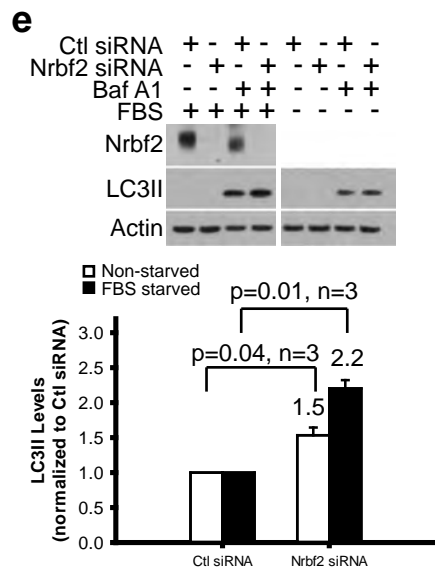
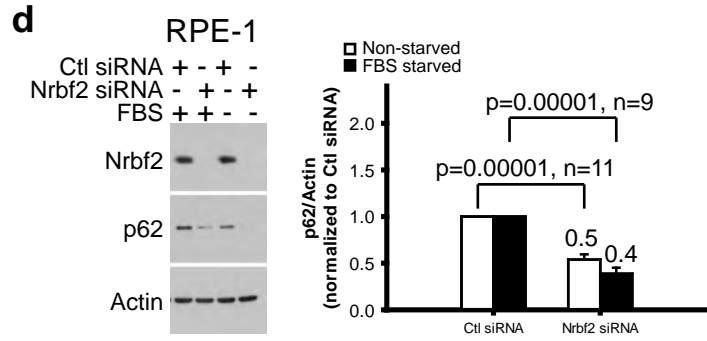
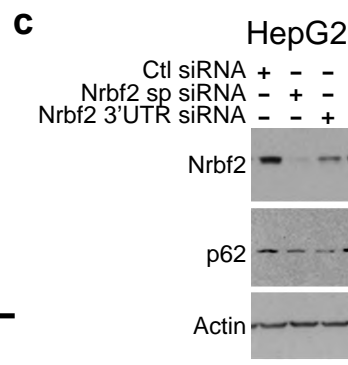
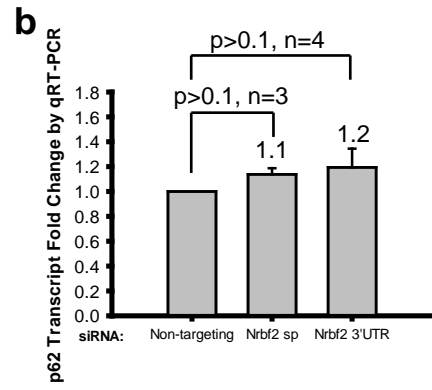
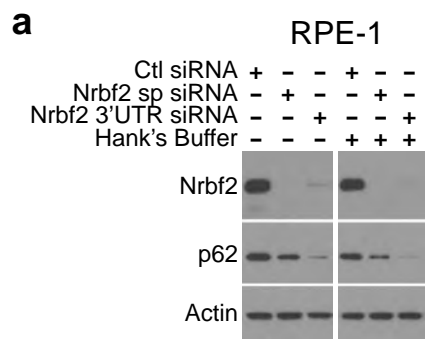


Figure 2

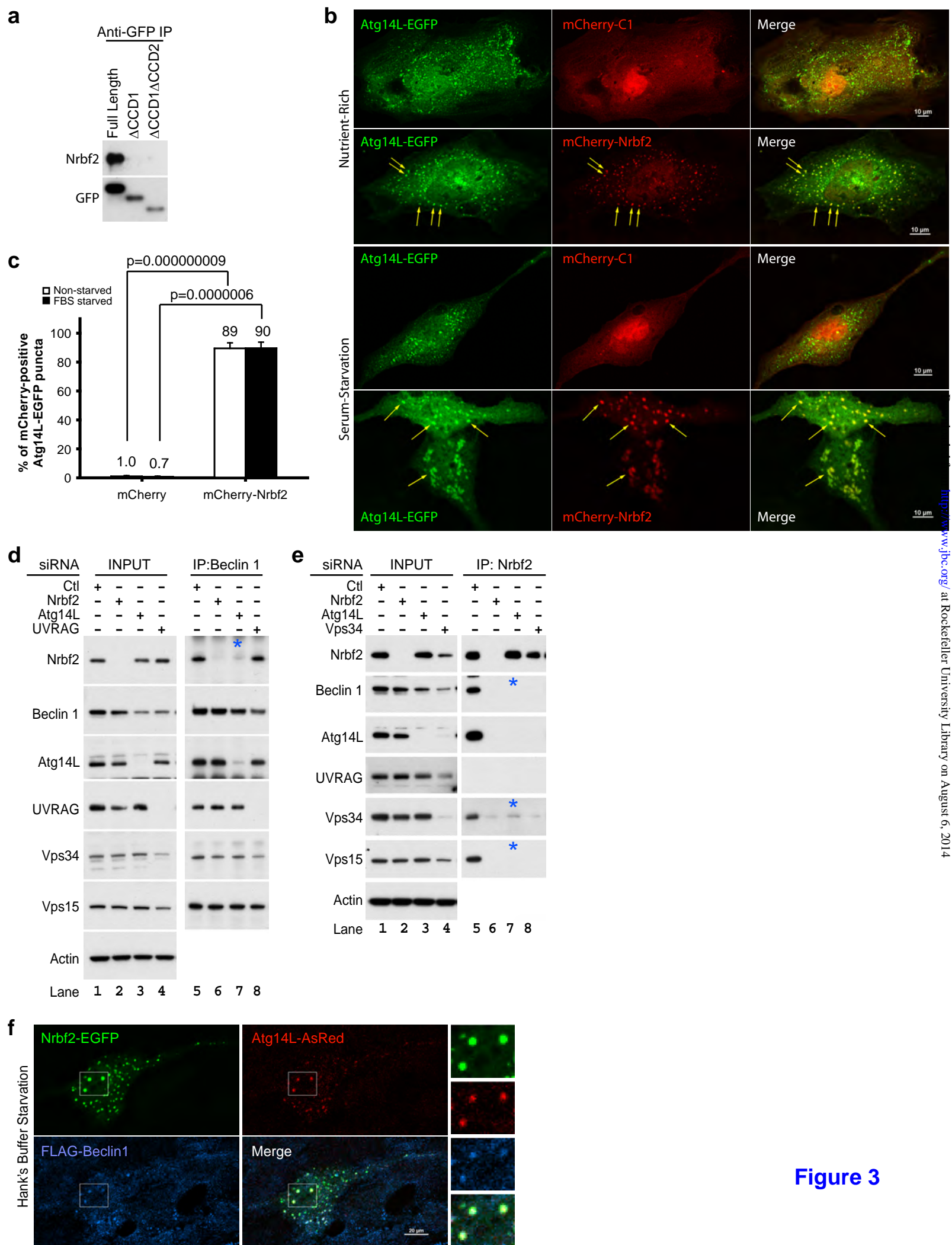
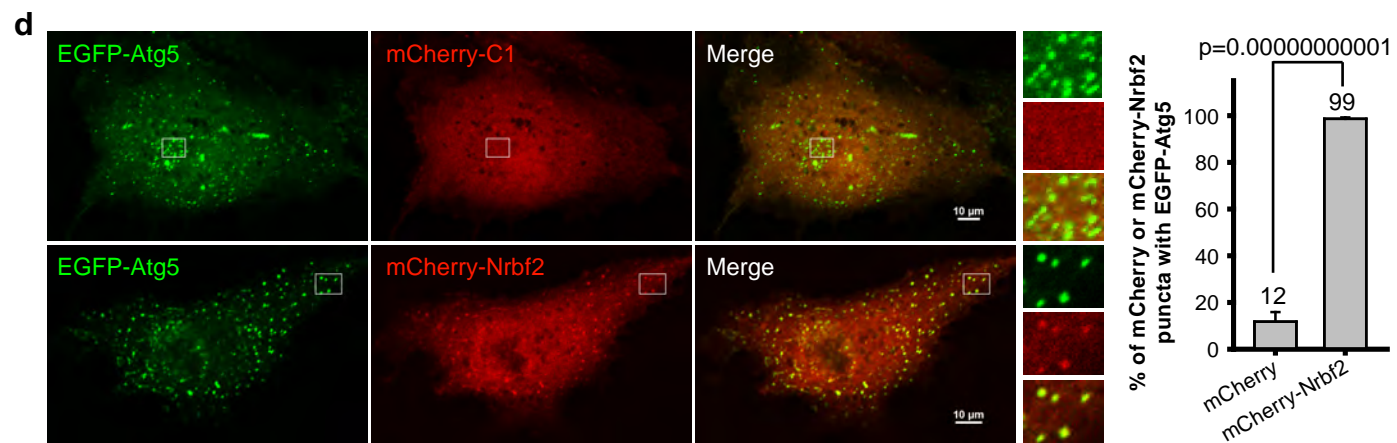
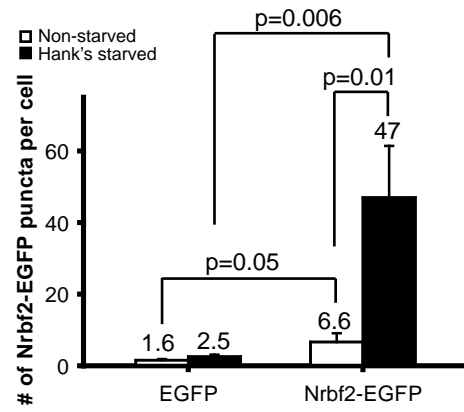
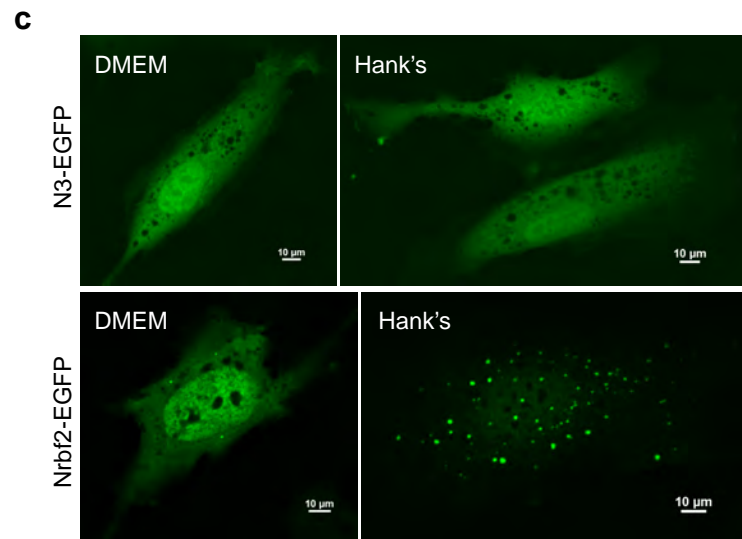
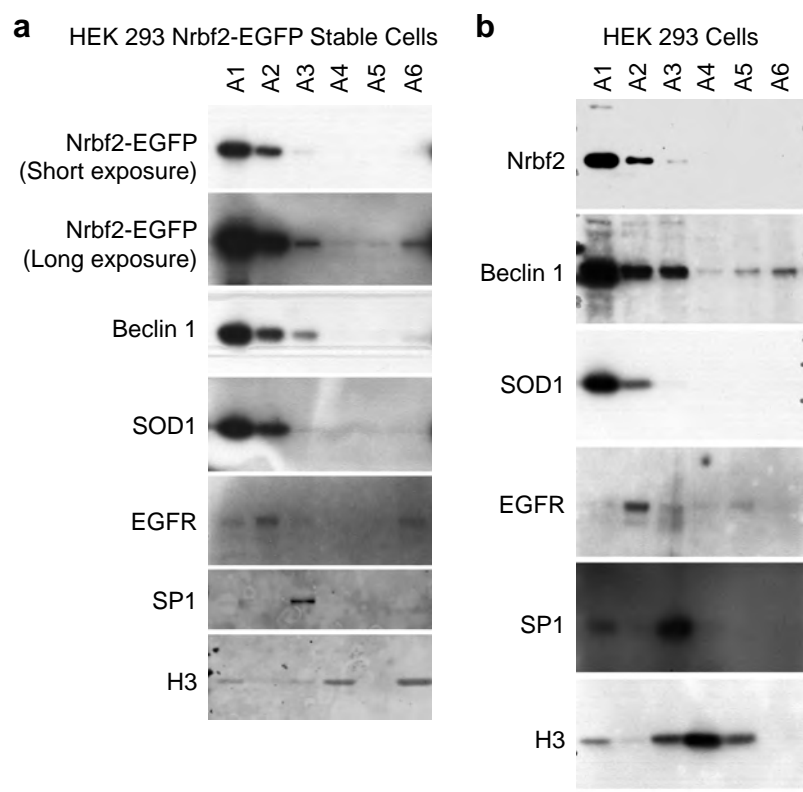
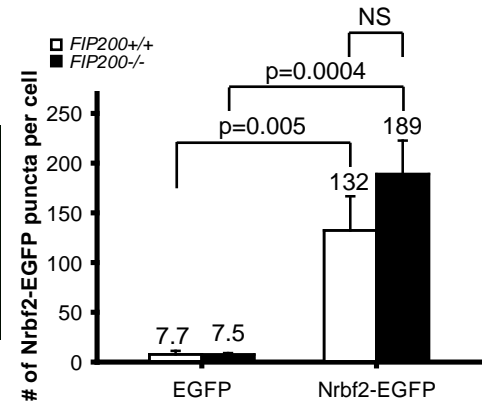
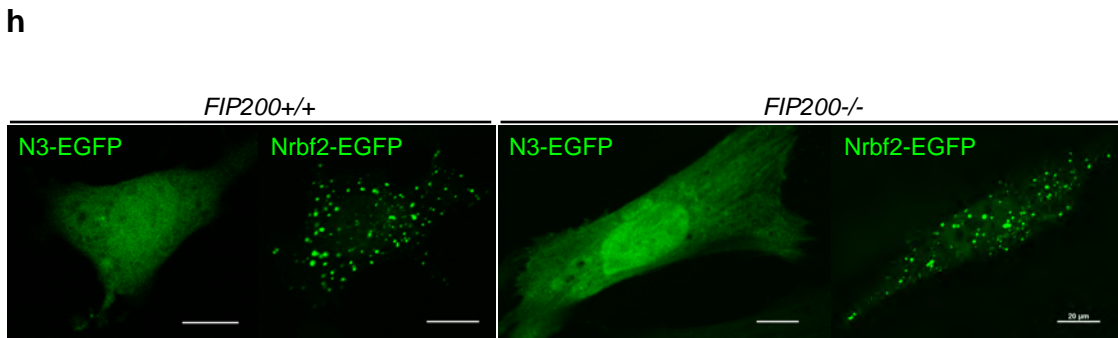
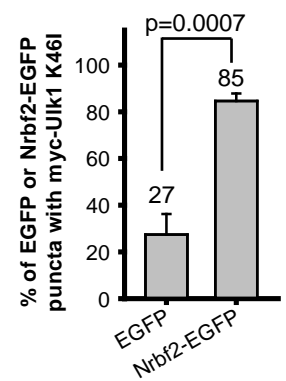
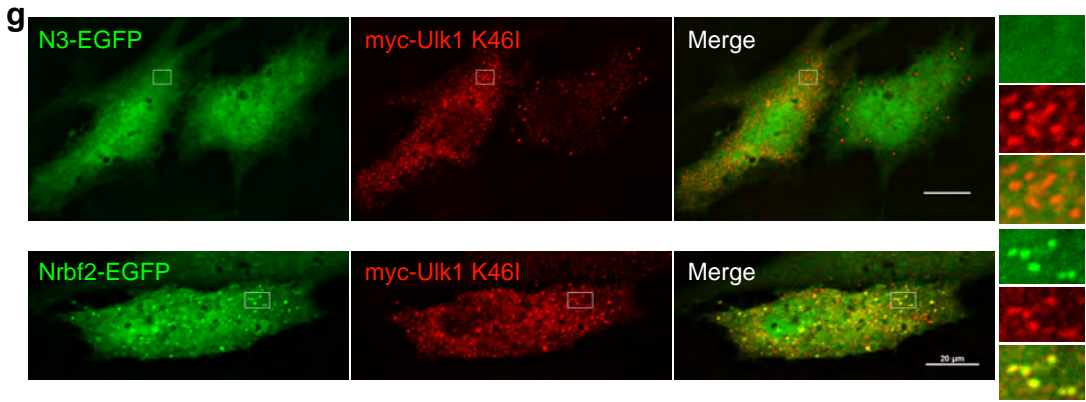
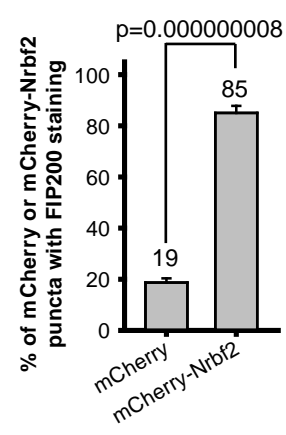
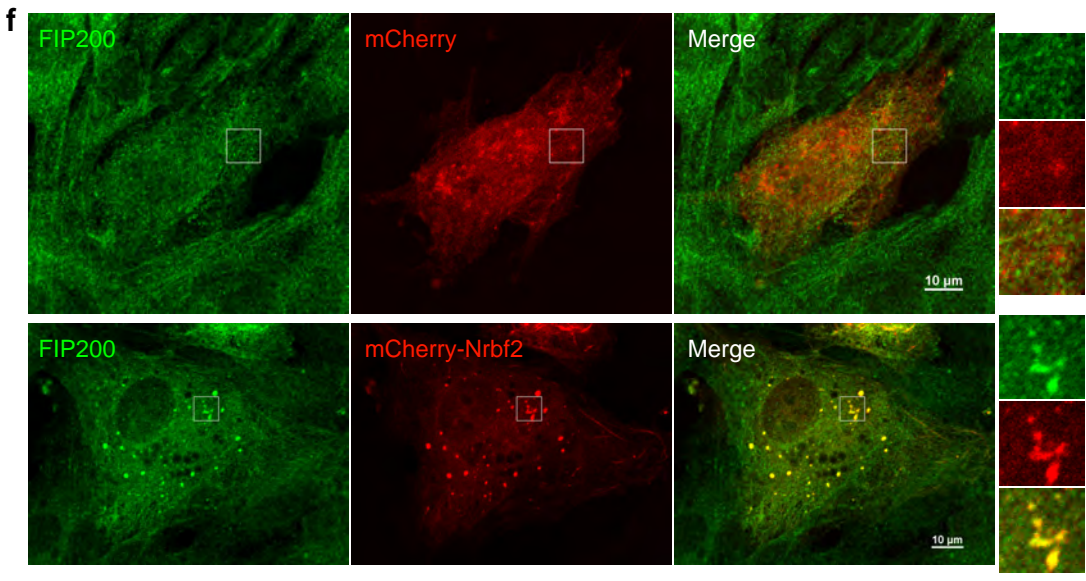
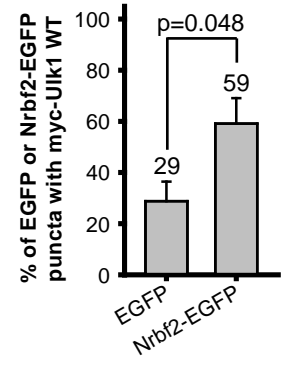
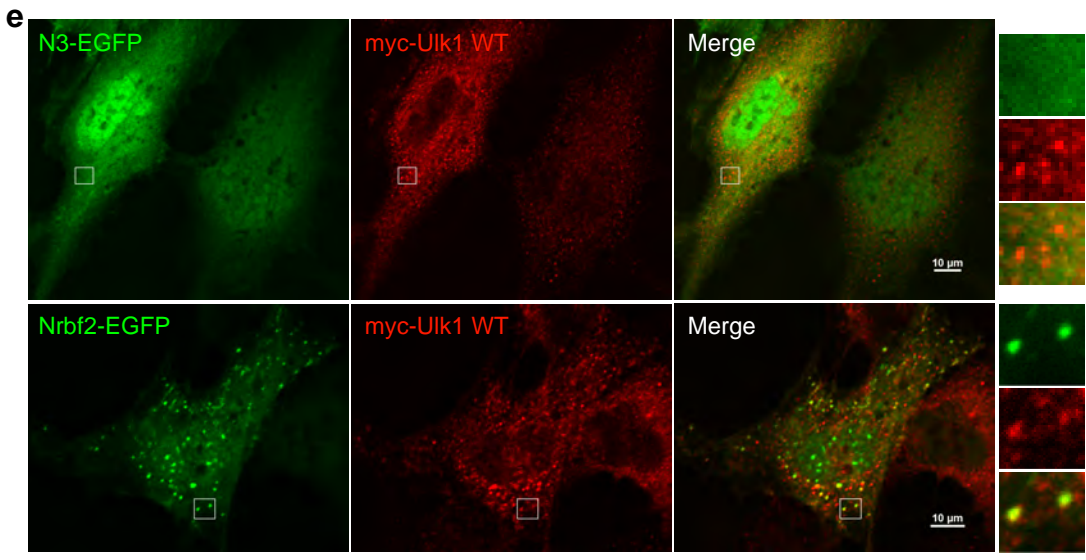


Figure 4-1





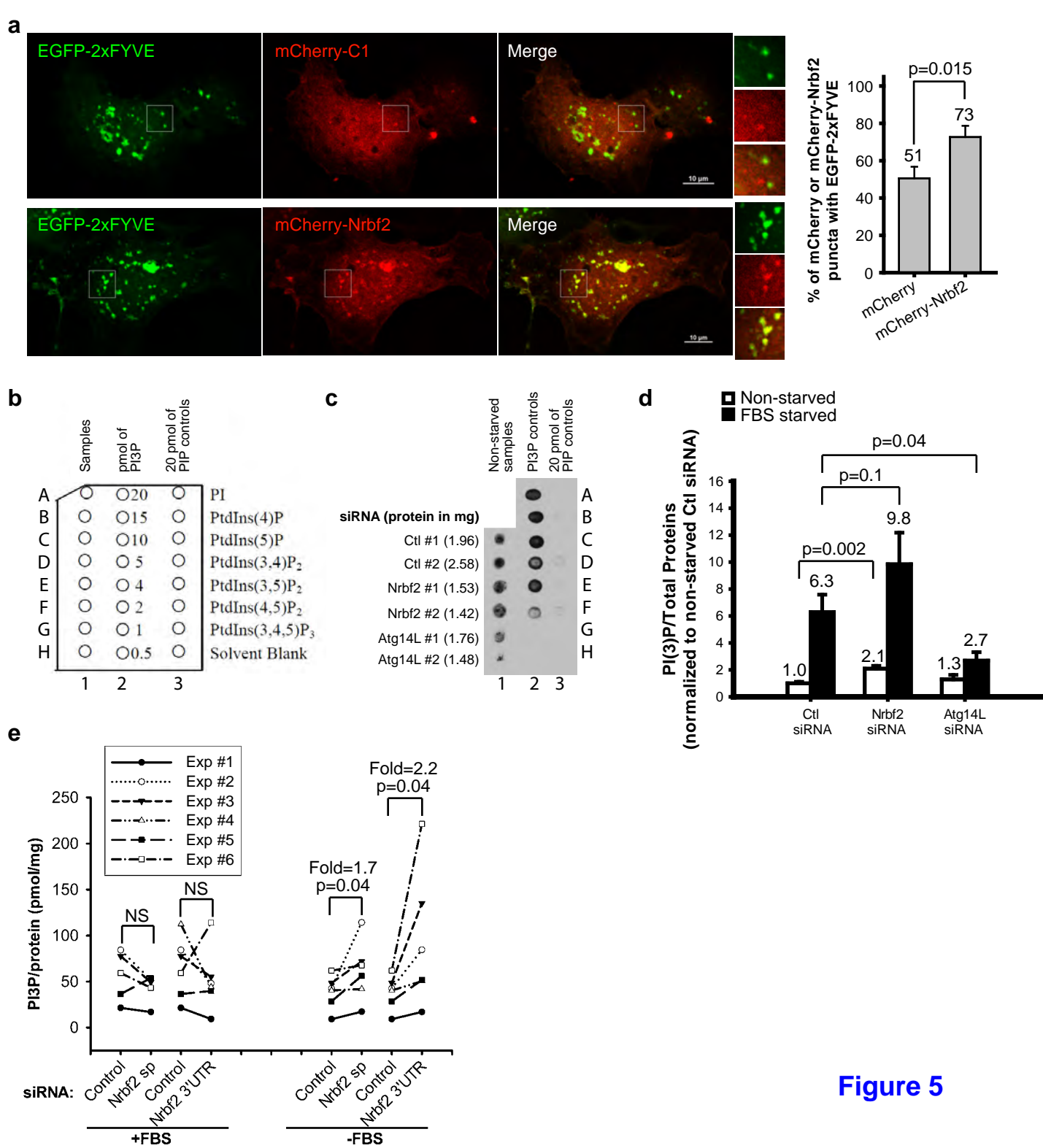


Figure 5

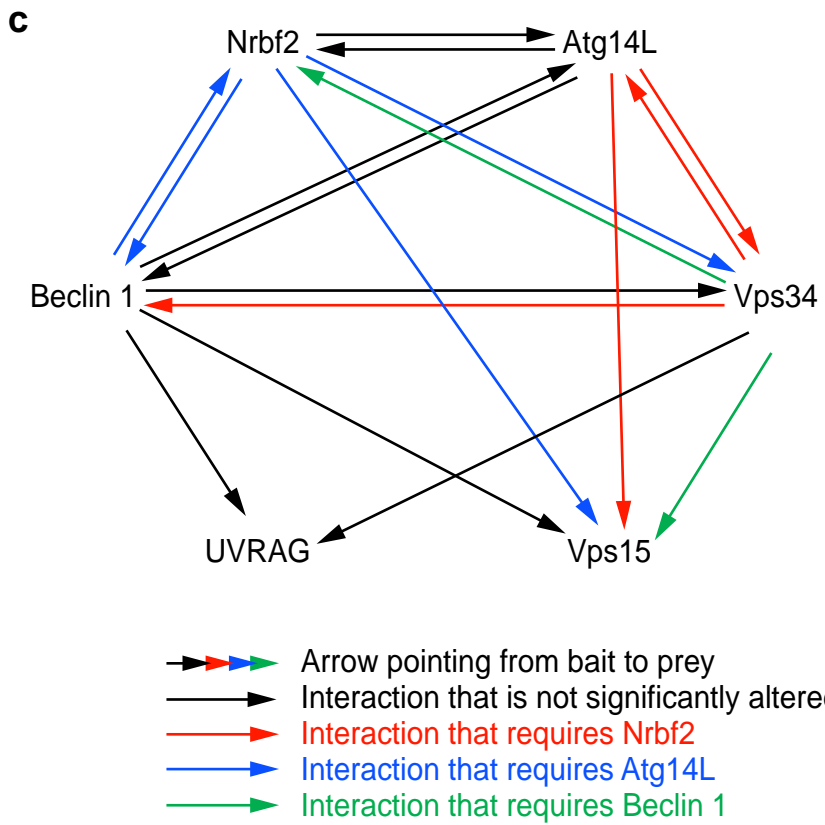
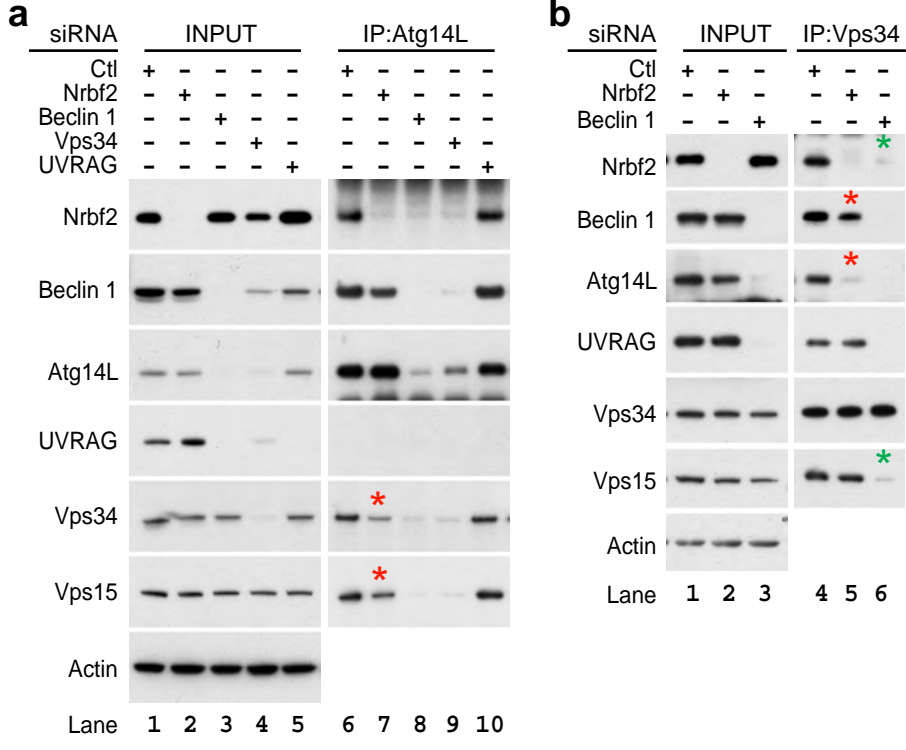


Figure 6